

# Coupled climate-glacier modelling of the last glaciation in the Alps

**Journal Article****Author(s):**

Jouvet, Guillaume; Cohen, Denis; Russo, Emmanuele; Buzan, Jonathan; Raible, Christoph C.; Haeberli, Wilfried; Kamleitner, Sarah; Ivy-Ochs, Susan; Imhof, Michael A.; Becker, Jens K.; Landgraf, Angela; Fischer, Urs H.

**Publication date:**

2023

**Permanent link:**

<https://doi.org/10.3929/ethz-b-000637778>

**Rights / license:**

[Creative Commons Attribution 4.0 International](#)

**Originally published in:**

Journal of Glaciology, <https://doi.org/10.1017/jog.2023.74>

**Funding acknowledgement:**

162444 - Modelling the ice flow in the western Alps during the last glacial cycle (SNF)



## Article

**Cite this article:** Jouvét G et al. (2023). Coupled climate-glacier modelling of the last glaciation in the Alps. *Journal of Glaciology* 1–15. <https://doi.org/10.1017/jog.2023.74>

Received: 9 January 2023

Revised: 20 July 2023

Accepted: 17 August 2023

**Keywords:**



glacier modelling; moraine; paleoclimate

**Corresponding author:**

Guillaume Jouvét;

Email: [guillaume.jouvet@unil.ch](mailto:guillaume.jouvet@unil.ch)

# Coupled climate-glacier modelling of the last glaciation in the Alps

Guillaume Jouvét<sup>1,2</sup> , Denis Cohen<sup>3,4</sup>, Emmanuele Russo<sup>5,6,7</sup>, Jonathan Buzan<sup>5,6</sup>, Christoph C. Raible<sup>5,6</sup>, Wilfried Haeblerli<sup>2</sup>, Sarah Kamleitner<sup>8</sup>, Susan Ivy-Ochs<sup>8</sup>, Michael A. Imhof<sup>9</sup> , Jens K. Becker<sup>10</sup>, Angela Landgraf<sup>10</sup> and Urs H. Fischer<sup>10</sup>

<sup>1</sup>Institute of Earth Surface Dynamics, University of Lausanne, Lausanne, Switzerland; <sup>2</sup>Department of Geography, University of Zurich, Zurich, Switzerland; <sup>3</sup>CoSci LLC, Orlando, FL, USA; <sup>4</sup>Department of Earth and Environmental Science, New Mexico Tech, Socorro, NM, USA; <sup>5</sup>Climate and Environmental Physics, University of Bern, Sidlerstrasse 5, 3012 Bern, Switzerland; <sup>6</sup>Oeschger Centre for Climate Change Research, University of Bern, Hochschulstrasse 4, 3012 Bern, Switzerland; <sup>7</sup>Institute for Atmospheric and Climate Science (IAC), ETH Zurich, Universitätsstrasse 16, 8092 Zürich, Switzerland; <sup>8</sup>Laboratory of Ion Beam Physics, ETH Zurich, 8093 Zurich, Switzerland; <sup>9</sup>Laboratory of Hydraulics, Hydrology and Glaciology, ETH Zurich, 8092 Zurich, Switzerland and <sup>10</sup>Nagra, Wettingen, Switzerland

**Abstract**

Our limited knowledge of the climate prevailing over Europe during former glaciations is the main obstacle to reconstruct the past evolution of the ice coverage over the Alps by numerical modelling. To address this challenge, we perform a two-step modelling approach: First, a regional climate model is used to downscale the time slice simulations of a global earth system model in high resolution, leading to climate snapshots during the Last Glacial Maximum (LGM) and the Marine Isotope Stage 4 (MIS4). Second, we combine these snapshots and a climate signal proxy to build a transient climate over the last glacial period and force the Parallel Ice Sheet Model to simulate the dynamical evolution of glaciers in the Alps. The results show that the extent of modelled glaciers during the LGM agrees with several independent key geological imprints, including moraine-based maximal reconstructed glacial extents, known ice transfluences and trajectories of erratic boulders of known origin and deposition. Our results highlight the benefit of multiphysical coupled climate and glacier transient modelling over simpler approaches to help reconstruct paleo glacier fluctuations in agreement with traces they have left on the landscape.

**1. Introduction**

The European Alps were characterised by multiple extensive glaciations (Ehlers and Gibbard, 2008) during the late Quaternary following glacial cycles of the Milankovitch theory. Our understanding of the most recent and most extensive glaciations is largely based on geomorphological evidence left on the landscape, such as moraines, erratic boulders, trimlines or drumlins (Kelly and others, 2004; Bini and others, 2009; Preusser and others, 2011; Palacios and others, 2021). In contrast, most of the geological traces related to earlier or less extensive glaciations were destroyed by subsequent glacier readvances. This is the reason why the Last Glacial Maximum (LGM, ~24'000 years BP in the Alps) and the deglaciation until the Holocene are the best constrained time periods during the late Quaternary (Ivy-Ochs, 2015; Ivy-Ochs and others, 2022). In fact, the extent of the Alpine Ice Field (AIF) is reasonably well defined in the Alpine forelands due to abundant moraines (Jäckli, 1962; Van Husen, 1987; Bini and others, 2009; Ehlers and others, 2011). Still, there are higher uncertainties in the timing of glacier advances (Kamleitner and others, 2022, Fig. 1), although cosmogenic nuclide dating has greatly improved our ability to assign an age to mapped features (e.g., Gosse and Phillips, 2001; Ivy-Ochs and Kober, 2008; Balco, 2011).

The European Alps are probably the place with the largest number of individual studies with precise mapping and dating of 15–20 lobes of the AIF (Wirsig and others, 2016, Fig. 5). Recent contributions have refined our knowledge by providing better time constraints, identifying multiphase LGM advances, as well as other maxima based on exposure age estimates of erratic boulders and other dating techniques (e.g. Graf and others, 2015, and references therein). These findings suggest that the Alpine glaciers during Marine Isotopic Stage 4 (MIS4, 71–59 ka BP) were generally less extensive than during the LGM. In the eastern Alps, there is no evidence of the presence of glaciers in the main Alpine valleys (van Husen, 2004), while in the western Alps an important glaciation reached the lowlands during MIS4 (e.g. Schlüchter, 1991). There are some hints that glacier extents larger than at the LGM may have occurred in the western Alps (e.g. the Lyon lobe Gribenski and others, 2021 or the Reuss Glacier Gaar and others, 2019). In the eastern Alps, the LGM appears to be the period with the maximal extent of glaciers, for example, in the Inn Valley (Spötl and others, 2013).

In recent years, numerical models that simulate the interaction between the thermodynamics of the ice and the climate-induced mass balance proved to be very valuable tools to deepen our understanding of glacial states from physical principles (Mey and others, 2016;



Jovet and others, 2017; Cohen and others, 2018; Seguinot and others, 2018; Imhof and others, 2019; Višnjić and others, 2020; Imhof, 2021). Among them, Seguinot and others (2018) simulated the evolution of the AIF at a resolution of 1 km during the entire last glacial cycle. The simulation suggests that the Alpine glaciers advanced several times on the foreland during this period. However, the uncertainty in climate forcing, which controls mass balance, and thus glacier extent, limits the scope of the results. Indeed, all of these studies – with the exception of Imhof (2021) – apply a distortion of today's climate to mimic paleo conditions, while several proxies (Florineth and Schlüchter, 2000; Luetscher and others, 2015; Monegato and others, 2017) suggest a dramatically different precipitation pattern over the Alps during the LGM (dominated by southerly atmospheric circulation) compared to today (dominated by westerly circulation). This may explain biases between model results and observations such as a too extensive glaciation in the east and a too weak extension of glaciers in the west (Seguinot and others, 2018), and the incorrect ice flow distribution between the Soluturn and Lyon lobes, as witnessed by trajectories of erratic boulders from the south Valais (Jovet and others, 2017).

Our current knowledge of the climate of glacial periods mainly relies on reconstructions from proxy records such as ice cores, speleothems, sediment cores, etc. For the midlatitudes of the northern hemisphere, pollen data are used mainly to generate reconstructions of temperature and precipitation (Bartlein and others, 2011; Cleator and others, 2020; Davis and others, 2022). For the LGM, these reconstructions indicate that the European climate was fundamentally different compared to the present-day (Mix and others, 2001). The temperatures were lower, with summer differences up to 6–12°C and winter ones up to 10–17 °C (Wu and others, 2007). Furthermore, reconstructed precipitation indicates that the LGM was probably dryer than today, but the amplitude of this reduction is rather uncertain. Indirect evidence of changes in atmospheric circulation during the LGM from the major loess deposits found across Europe (Antoine and others, 2009; Obrecht and others, 2019) and from several independent proxy-based studies of LGM precipitation (Florineth and Schlüchter, 2000; Luetscher and others, 2015; Monegato and others, 2017), suggest that LGM precipitation was mainly controlled by south-westerly flow, whereas today's precipitation is advected from the west-northwest direction (Fig. 1).

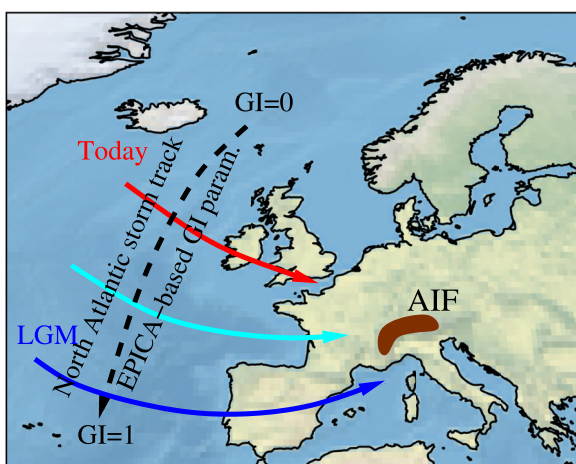


**Figure 1.** The North-Atlantic storm track and the resulting moisture advection towards and across the Alps were probably shifted southwards at the LGM compared to present-day conditions. The glacial index parametrisation used in this study can be seen as a control of the North-Atlantic storm track: the moisture is mostly advected towards the north west of the Alps when GI is close to zero to mimic present-day situation, while the moisture advection is shifted southwards when GI is close to one to mimic the LGM situation.

Physically consistent climate models complement our understanding of the relevant processes governing the climate of glacial periods by filling existing gaps of spatial coverage and temporal resolution of proxy data (Raible and others, 2021). Additionally, models constitute a powerful tool for testing plausible physical hypotheses for the interpretation of evidence from proxies (Russo and others, 2022). Hence, the global LGM is one of the key periods selected by the Paleo Modelling Intercomparison Projects (Kageyama and others, 2021). Models helped identify atmospheric circulation changes during the LGM (Kutzbach and Geuetter, 1986; Dong and Valdes, 1998; Kageyama and others, 1999; Hofer and others, 2012b, 2012a; Merz and others, 2015; Lofverstrom and others, 2016). For example, Merz and others (2015) provided evidence that the stationary wave activity is enhanced southeast of the Northern Hemisphere Ice Sheet (NHIS) during glacial periods. The consequential southward shift of the storm track and the jet stream (Fig. 1), strongly affects the precipitation pattern over the north Atlantic and Europe (e.g., Hofer and others, 2012b; Lofverstrom and others, 2016; Roberts and others, 2019).

Yet, these global modelling approaches allow to resolve processes at relatively coarse resolutions, between 100 and 200 km. This is a strong limitation, in particular over complex terrain such as the Alps. To increase resolution, global climate model simulations are statistically (Latombe and others, 2018) or dynamically downscaled (Prömmel and others, 2013; Fallah and others, 2016; Russo and Cubasch, 2016; Ludwig and others, 2017; Fallah and others, 2018; Russo and others, 2022). Del Gobbo and others (2023) used a regional climate model (RCM) to reconstruct the equilibrium line altitude (ELA) of glaciers in the Alps at the LGM. They found consistent results with geologically based glacier extent reconstructions, demonstrating the potential of climate modelling, especially the patterns of paleo precipitation which play an important role in the distribution of ice. However, this study had two limitations: (i) The low resolution of the climate model (12 km) can hardly resolve the mountain orography in the Alpine environment, (ii) their ELA-based glacier reconstruction lacks essential transient and dynamical aspects of the climate–glacier interactions. Recently, a convection-permitting regional climate was applied to realistically represent precipitation-related processes over the Alps, during glacial periods such as the LGM and MIS4 (Velasquez and others, 2020, 2021, 2022; Russo and others, 2023). These new achievements in climate modelling enable us to provide physically consistent high-resolution boundary conditions for glacier modelling over the Alps.

In this paper, we attempt to overcome the two aforementioned limitations, and present a reconstruction of the AIF over the last 120 000 years by combining state-of-the-art, high-resolution (2 km), RCM obtained with the Weather Research and Forecasting Model (WRF, Powers and others (2017)), and glacier modelling with the Parallel Ice Sheet Model (PISM). Our study follows the work of Seguinot and others (2018) and Imhof (2021), but uses a modelled paleoclimate instead of a distortion of present-day climate for forcing the AIF mass balance in PISM. This new approach yields an improved match between LGM-related characteristics, such as maximal extent, ice flow and ice thickness, with field evidence observations.

The outline of this paper is as follows. First, we describe the climate and glacier models. Then we present the new AIF for the last glaciation cycle and compare the simulation with documented geological field evidence. Finally, we discuss the implications of our new findings for our knowledge of the AIF.

## 2. Models

To simulate the AIF over paleo-time scales with a resolution that allows to capture the complex topography of the alpine mountain

range, we first target a series of climate states by combining global Earth System (ESM) and Regional Climate Models (RCM) following an approach already applied by Velasquez and others (2020, 2021, 2022). Then, we generate a transient climate using a Glacial Index (GI) approach. Finally, we use the transient climate to force the Parallel Ice Sheet Model (PISM). These four key steps are illustrated in Figure 2.

2.1. Earth System Model (ESM)

The Community Earth System Model (CESM, version 1.2 Hurrell and others, 2013) is used to perform simulations for key periods (referred as ‘states’) during the late Quaternary. We use the fully coupled version of the model with a coarser resolution of ~2° in the atmosphere and 1° in the ocean. The original LGM state is derived from a 1500-year-long simulation (Zhu and others, 2017). This was extended an additional 150 years and then subsequent sensitivity simulations are run to reach a quasi-equilibrium state (this takes ~400 years depending on the climate state and the initial conditions used). Then we repeat the simulation using only the atmospheric and land model components, with an increased horizontal resolution of 0.9° × 1.2°, using prescribed time-varying sea surface temperatures and sea-ice distributions obtained from the fully coupled simulation. This strategy is applied to the Pre-Industrial (PI) period, the global LGM (~21 ka) and the MIS4 (~65 ka) (Buzan and others, 2023). Throughout the paper, the LGM climate state refers implicitly to the global LGM (~21 ka) while the LGM in the Alps (i.e. the timing of maximum glaciation) refers to ~24 ka. The climate forcing of the states consists of changes in orbital parameters, concentration of greenhouse gases and prescribed reconstructed NHIS configurations for LGM and MIS4. As studies have shown that the NHIS plays an important role in shaping the climate of Europe during glacial periods (Merz and others, 2015), we perform a set of sensitivity simulations for each of the LGM and MIS4 glacial states, scaling the height of the NHIS (Fig. 1 in Buzan and others, 2023) by 66, 100 and 125% of the reconstruction of Peltier and others (2015). Indeed, Batchelor and others (2019) estimates that the ice heights are up to 125% (MIS6) and down to 67% (MIS8/MIS4), therefore, our three simulations cover a physical range of uncertainty. Thus, in total, we have seven global model simulations available. Further technical details on the global simulations performed are presented in Buzan and others (2023).

2.2. Regional Climate Model (RCM)

The ESM simulations are the basis for the second step in the model chain (Fig. 2), the dynamical downscaling. For this purpose, we use the Weather Research and Forecasting model (WRF, version 3.8.1) (Skamarock and others, 2008; Powers and others, 2017). The model uses four two-way nested domains,

with a spatial resolution going from 54 km over Europe, down to 2 km over the Alps. In the two innermost domains, the convection parametrisation is switched off, leading to a more realistic simulation of precipitation (Ban and others, 2014; Messmer and others, 2017; Velasquez and others, 2020). For the different glacial periods, the RCM requires information on the top surface elevation (the AIF) at the time of the considered state, which is not available a priori as this is what we intend to model. Instead, we use as ice surface topography input for the model over the Alpine region, the LGM ice surface topography derived from an earlier modelling work, for all states except for the PI for which the present-day surface topography is taken. Similarly, we use the maximum top surface elevation of the Fennoscandian ice sheet from 24 to 18 ka BP from the dataset of Peltier and others (2015) to force the RCM at a continental scale. Each of the seven simulations is performed for 10 years in order to obtain mean values necessary for the subsequent glacier modelling with PISM. More details on the parametrisations used, the necessary model developments to make the model usable for paleo applications and the assessment of model performances against proxy reconstructions are presented in Russo and others (2023).

In summary, the climate model chain provides physically consistent high-resolution (2 km) values of temperature and precipitation fields at daily timescales over 10 years for each targeted climate state (PI, LGM, MIS4). Because such a high temporal resolution is not needed for glacier modelling, we calculate, for each period, decadal monthly averages of daily values of temperature and precipitation. To keep the annual and daily variability of the original temperature data, we additionally estimate the monthly standard deviation of the mean daily temperatures. Note that the temperature fields always refer to the surface topography given as input to the RCM, which is the same for all states except for the PI. To simulate the temperature when the modelled surface deviates from the reference one, we apply a vertical and linear lapse correction, the lapse rate being estimated from the RCM outputs to 6 and 5.74 °C km<sup>-1</sup> for the PI and LGM/MIS4 states, respectively.

2.3. Glacial index approach

To extend the climate data between the states, we adopt a GI approach (e.g. Sutter and others, 2019). For this purpose, we define a function GI that maps time *t* to a scalar with two extreme states: one state with almost no ice over the Alps corresponding to GI=0 and one maximum state in terms of glacier extent corresponding GI=1. The climate CL consists of a set of variables: mean temperature, temperature variability, mean precipitation and lapse rate,

$$CL(t) = (T^{mean}(t), T^{std}(t), P^{mean}(t), LR(t)), \tag{1}$$

and is assumed to be a linear combination:

$$CL(t) = GI(t) \times CL_1(t) + (1 - GI(t)) \times CL_0(t), \tag{2}$$

where the two climate states

$$CL_0(t) = (T_0^{mean}(t), T_0^{std}(t), P_0^{mean}(t), LR_0(t)), \tag{3}$$

$$CL_1(t) = (T_1^{mean}(t), T_1^{std}(t), P_1^{mean}(t), LR_1(t)), \tag{4}$$

correspond to GI=0 and GI=1, respectively. Here, we associate the Pre-Industrial (PI) climate state with GI=0:

$$CL_0(t) = CL_{PI}, \tag{5}$$

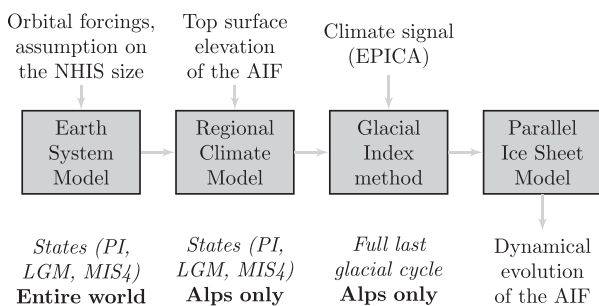


Figure 2. Model chain implemented in the study.

and MIS4 and LGM with  $GI=1$  as follows:

$$CL_1(t) = \begin{cases} CL_{MIS4}, & \text{if } -120 \text{ ka} \leq t \leq -45 \text{ ka}, \\ CL_{LGM}, & \text{if } -45 \text{ ka} \leq t \leq 0. \end{cases} \quad (6)$$

Last, the GI function is built by linearly rescaling a climate proxy signal in such a way that GI is close to 1 at the LGM and close to 0 at the PI. The chosen procedure is used to build the AIF consistently with geomorphological evidence (especially in the building phase of the LGM) but can, of course, not reproduce the full timing and complexity of the last glacial cycle climate. Despite its distance to the AIF, we mainly used here the Antarctic EPICA temperature anomaly signal (Jouzel and others, 2007), which is available for the last 800 000 years, because it yields the best match with geological evidence and a realistic global timing of the maximum glacier extent among the three signals tested. These include EPICA, the Greenland NGRIP signal (Seierstad and others, 2014) and a local pollen-based signal (rescaled linearly from the principal component of the pollen data) from Bergsee, southern Germany (Duprat-Oualid and others, 2017). For sensitivity analysis, we also show results obtained with the Bergsee signal, which is available from 45 to 15 ka BP. The two resulting GI functions are shown in Figure 3, top panel. Note that we, in fact, rescaled the EPICA signal to slightly negative GI values ( $\sim -0.25$ ) at the PI to correct for an overestimation of modelled ice volumes during the Holocene obtained when rescaling the GI to zero. We mainly attribute this bias to (i) an inadequacy of the model resolution (2 km) to resolve Holocene/present-day small-scale glaciers (the tongue of the largest present-day glacier being narrower than one pixel resolution, leading to underestimated ice flow, and thus artificial ice accumulation), (ii) biases in PI modelled climate and (iii) inappropriate melt parameters. Due to (i), we refrain from analysing the results of our model during the Holocene.

#### 2.4. Parallel Ice Sheet Model (PISM)

We use the Parallel Ice Sheet Model (PISM, Bueler and Brown, 2009; Winkelmann and others, 2011) (version 2.0.2), which jointly models the ice thickness evolution, the ice

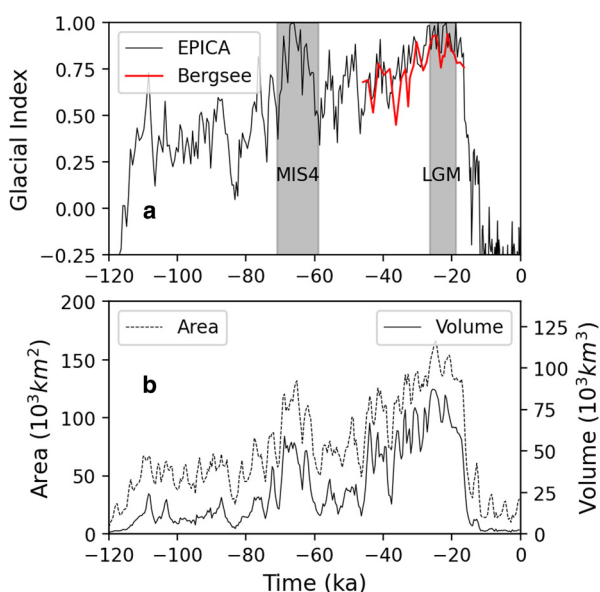


**Figure 3.** Time evolution of the glacial index based on the EPICA (continuous line) and Bergsee (dashed line) signals for climate forcing (continuous line, panel a), and resulting modelled evolution of the entire glaciated area and ice volume (panel b) during the last glacial cycle (based on EPICA).

thermodynamics, the surface mass balance, and the deformation of the lithosphere given initial conditions (Fig. 4). The four model components of PISM are described in turn.

1. To model the dynamical motion of ice, PISM uses a linear combination of low order approximations (Bueler and Brown, 2009), namely the shallow ice approximation (SIA) for the vertical shear and the shallow shelf approximation (SSA) for the longitudinal ice extension. This hybrid approach is a trade-off between mechanical accuracy and computational cost that permits to simulate long time scales. In the SSA, the basal velocity and the basal shear stress are related non-linearly with the Mohr–Coulomb sliding law (Cuffey and Paterson, 2010). This law is parameterised by the yield stress, i.e. the product of the till friction angle and the effective pressure in the till, which is determined by the weight of the ice column minus the modelled pressure of water in the till derived from a simple subglacial hydrology model (Khroulev and the PISM Authors, 2022).
2. PISM is a polythermal model, i.e. it solves jointly the ice dynamics together with the ice temperature field in three dimensions using an enthalpy formulation (Aschwanden and others, 2012). The ice enthalpy (or the temperature and the water content) impacts both the ice softness, as well as the basal motion. Additionally, the dynamics of ice influences the evolution of the enthalpy field. The enthalpy equation is constrained by the mean air temperature at the glacier surface (given by the climate forcing) and by a spatially variable geothermal heat flux at the glacier base (here we use the data of Goutorbe and others (2011)).
3. PISM uses a combined snow accumulation/positive degree-day (PDD) model (cf. Hock, 2003) to compute the surface mass balance from temperature and precipitation fields. On the one hand, surface accumulation is equal to solid precipitation when temperature is below  $0^\circ\text{C}$ , and decreases to zero linearly between  $0$  and  $2^\circ\text{C}$ . On the other hand, the surface ablation is computed proportionally to the number of PDD. The PDD integral is numerically approximated using week-long sub-intervals based on Calov and Greve (2005), with PDD proportionality factors of  $f_i = 8 \times C \text{ mm } ^\circ\text{C}^{-1} \text{ day}^{-1}$  for ice, and  $f_s = 3 \times C \text{ mm } ^\circ\text{C}^{-1} \text{ day}^{-1}$  for snow, where  $C$  is a tuning parameter. Note that a fraction (60%) of the melt is assumed to refreeze. These values coincide with the ones of the EISMINT intercomparison experiments for Greenland (MacAyeal, 1997) when  $C = 1$ . Note that PDD parameters are not well constrained and may vary substantially:  $C \in [0.5, 2]$  encompasses most values measured in Greenland (e.g. Braithwaite, 1995; Braithwaite and Zhang, 2000), and the values used by Heyman and others (2013) to model LGM surface mass balance in central Europe. Therefore, the parameter  $C$  is used to tune the modelled maximum extent to the LGM maximum observed extent.
4. PISM includes an Earth deformation model based on Lingle and Clark (1985) and Bueler and others (2007), which combines a layered elastic spherical Earth with a viscous half-space overlain by an elastic plate lithosphere.

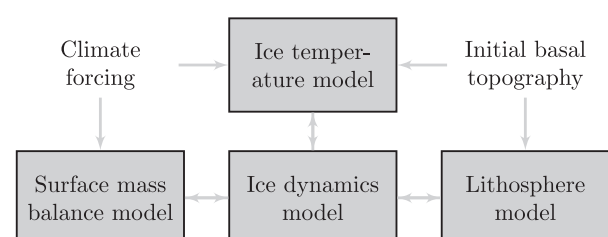


**Figure 4.** Flowchart of PISM model components.

For climate forcing, several possible scenarios are available based on (i) the choice of the height of the NHIS, 66 100 or 125% of the height of the NHIS where 100% is the height of the NHIS computed by Zhu and others (2017), and (ii) the climate proxy signal for the GI method (EPICA available over the entire last glacial period or Bergsee available from 45 to 15 ka BP, Fig. 3). In this paper, we focus mainly on one simulation obtained using NHIS 66% and the EPICA climate signal, since this combination gives the best geological reconstruction of the glacial extent at the LGM both temporally and spatially. However, the sensitivity of the different climate forcings is tested in additional simulations. Also, the sensitivity to the thermal component of the ice dynamical model is investigated.

To simulate the evolution of the AIF, we build an initial basal topography using the publicly available NASA Shuttle Radar Topographic Mission (SRTM, <http://srtm.csi.cgiar.org/>) Digital Elevation Model (DEM), re-sampled at 2 km resolution, and remove major lakes (e.g. Lake Constance and Lake Zurich) and present day glaciers (Farinotti and others, 2019). The simulation is initialised with ice-free conditions at 120 ka BP. Note that the modelling results are not affected by the initialisation procedure, as the response time of the AIF does not exceed a few millennia. The melt control parameter,  $C$ , is calibrated such that the glacial maximum area best fits the reconstructed value given by Ehlers and others (2011). The settings in PISM for the thermodynamical and bed deformation models are identical to the ones of Seguinot and others (2018) and Mey and others (2016), respectively.

### 3. Results and discussion

In this section, we first discuss the results of the modelled climate states. Then we analyse the modelled glacier fluctuations and the timing of the global maxima before conducting a regional analysis of several glacier lobes of the AIF, comparing modelled outcomes with geological reconstructions. We then analyse the ice thickness and flow within the Rhone catchment and discuss the findings against field evidence. Sensitivity analyses are reported to assess the influence of key climatic and non-climatic model parameters. Lastly, we compare our results with previous modelling studies, and discuss the benefits of coupled climate and glacier modelling for paleo-glacier reconstruction in the Alps. As our model was primarily designed to match LGM evidence, our analysis focusses primarily on maximum states, and to a lesser extent the intermediate states. As explained before, our model resolution (2 km) is not suitable for modelling glacier extent during the Holocene. Therefore, this period is excluded from the analysis.

#### 3.1. PI, LGM and MIS4 climate states

Figure 5 shows the modelled PI and LGM NHIS 66% climate states summer temperature and winter precipitation, two first-order control variables of the surface mass balance of a glacier. Simulated LGM climate conditions are substantially colder (by 12.5°C in summer, 12°C annually) on average compared to the PI period. Note that the temperature difference includes the important change in surface elevation: at the LGM, the surface topography is substantially higher than at PI due to the presence of the AIF, which amplifies the temperature decrease by several degrees. As expected, the precipitation pattern at the LGM differs substantially from PI and indicates overall drier conditions, on average about 17% in winter and 21% annually.

Figure 6 shows the difference between LGM and MIS4 for summer temperature and winter precipitation. We find that the MIS4 is slightly warmer (~2.5°C in summer, ~0.5°C annually) than the LGM, especially in the southern Alps, while it is slightly

drier (~15% in winter, ~5% annually) than the LGM, especially in the northern part of the Alps.

Lastly, Figure 7 shows the variations between the climate variables obtained under the scaling assumptions of NHIS 66% and NHIS 100%. A NHIS 100% leads to warmer temperatures (~0.6°C in summer, ~1.2°C annually) and less precipitation (~22% in winter, ~2% annually) compared to 66% NHIS. The precipitation pattern is also affected by the NHIS scaling parameter: the 100% NHIS climate has more precipitation south of the Alps compared to 66% as expected since the 66% NHIS can be seen as an intermediate state between PI (no NHIS) and 100%. Note that we find (not shown) that changing from a 100% to a 125% NHIS has only a minor impact on the climatic conditions modelled in the Alps. Comparison of climate model outputs with recently available pollen-based reconstructions (Davis and others, 2022) is performed by Russo and others (2023).

#### 3.2. Compatibility climate/glaciation

When tuning melt parameters in the iceflow model to reproduce the geomorphologically reconstructed glacier outlines (Fig. 8), we find that only a minor ( $C = 1.1$ ) adjustment was needed, i.e. the melt parameters needed to be increased by only 10% from the values of the EISMINT intercomparison experiments (MacAyeal, 1997), which are standard mean values from the literature. Furthermore, the maximum extent of the east-west glaciers modelled matches (Fig. 8) the geomorphological reconstruction of Ehlers and others (2011) fairly well. This result supports the adequacy of the chain of data and models (Fig. 4) and the minor adjustment of the PDD parameter  $C$  shows the general compatibility of the climate and glacier models.

#### 3.3. Glacier fluctuations and timing of maxima

Similarly to Seguinot and others (2018), our simulation suggests that the size and extent of the AIF fluctuated during the last glacial cycle with many advance and retreat phases onto the Alpine foreland (Fig. 9) and two distinct periods of extensive glaciations: a first maximum occurs during MIS4 reaching a maximum ice volume of  $\sim 67 \times 10^3 \text{ km}^3$  at  $\sim 68 \text{ ka}$ ; a second maximum occurs during LGM reaching a maximum ice volume of  $\sim 88 \times 10^3 \text{ km}^3$  and a glaciated area of  $\sim 167 \times 10^3 \text{ km}^2$  at  $\sim 25 \text{ ka}$  (Fig. 3). Most glaciers reached their maximum thicknesses close to the LGM (between 30 and 20 ka, Fig. 10), and the largest glaciers were significantly smaller during MIS4 compared to the LGM (Fig. 11).

Fluctuations are clearly controlled by the size of the catchments and the resulting inertia of each glacier (Figs 9 and 12). The largest glacier located in the western Alps, the Rhone Glacier and its two lobes, the Lyon and Solothurn lobes, shows a single, long and late advance ( $\sim 23 \text{ ka}$ ) into the foreland. On the contrary, the medium-sized Rhine Glacier exhibits multiple, shorter and slightly earlier ( $\sim 24 \text{ ka}$ ) maxima. This situation is even more pronounced with other smaller glaciers in the east and in the south of the Alps (e.g. Ticino-Toce, Tagliamento).

#### 3.4. Individual glacier lobes

In this section, we analyse glaciers individually starting with the Rhine Glacier and looping around the Alps counterclockwise (Fig. 8).

##### 3.4.1. Rhine Glacier

Our simulation shows that the Rhine Glacier may have advanced multiple times into the foreland during MIS4 and LGM (about 10 times in total, Fig. 9). Despite an overshoot of at most 15 km at

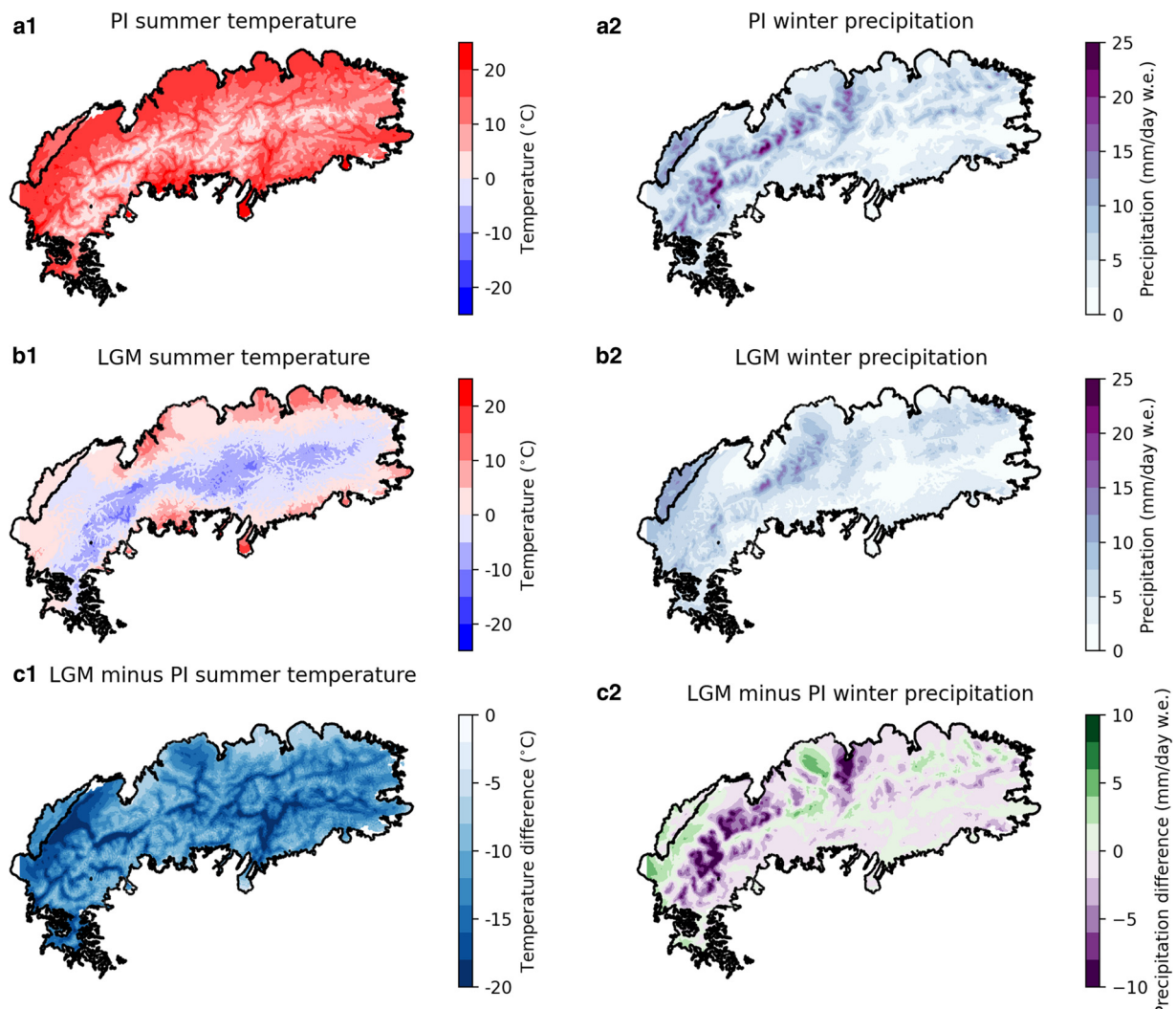


**Figure 5.** Summer temperature (panels a1–c1) and winter precipitation (panels a2–c2) of the modelled PI (panels a) and LGM (panels b) over the Alps. Panels c show the difference between LGM and PI.

LGM (Figs 8 and 9), the modelled LGM and post-LGM periods are well in line with spatio-temporal reconstruction based on geomorphological mapping and cosmogenic nuclide, luminescence and radiocarbon ages for the different ice-marginal positions (Preusser and others, 2007; Kamleitner and others, 2023). In particular, Figure 9 shows that the double maximum and the post-LGM deglaciation are well reproduced by the model. Geomorphologically, the former is seen as the Schaffhausen and Stein am Rhein stadal moraine complexes, dated 26–22 and  $20.6 \pm 1.7$  ka, respectively (Kamleitner and others, 2023).

#### 3.4.2. Reuss Glacier

According to luminescence ages from Gaar and others (2019), Reuss Glacier reached its maximum extent around  $24/25 \pm 2$  ka. In total, four stadials have been identified (Untertannwald, Mellingen, Stetten, Bremgarten) with clear signs of glacier readvances for Mellingen and Bremgarten stadials (Kamleitner and others, 2023).  $^{10}\text{Be}$  exposure ages suggest abandonment of the Reuss LGM maximum position was underway by  $22 \pm 1$  ka (Reber and others, 2014; Kamleitner and others, 2023). The Bremgarten stadal moraines were built after  $20.8 \pm 1.3$  ka

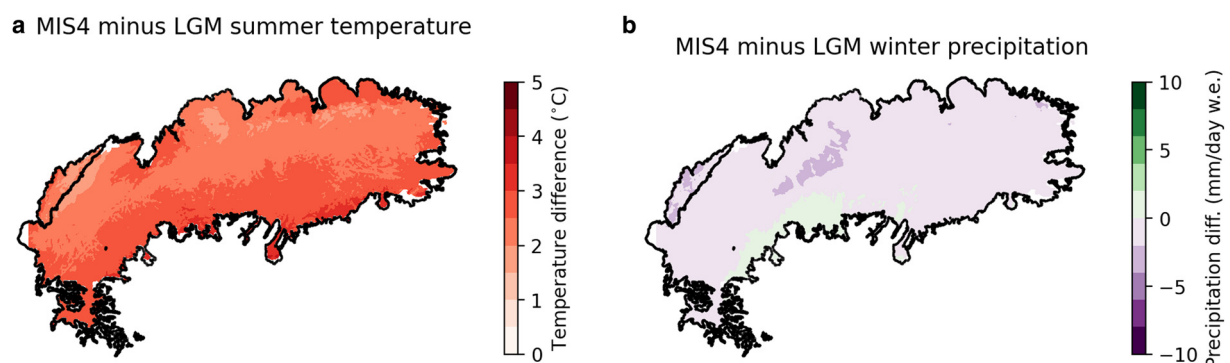


**Figure 6.** Difference between summer temperature (panel a) and winter precipitation (panel b) of the modelled climate values between MIS4 and LGM.

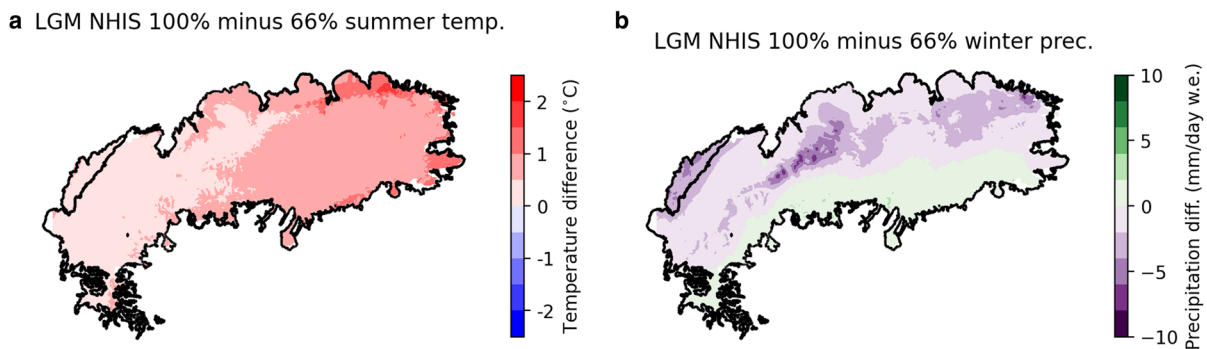


**Figure 7.** Difference between summer temperature (panel a) and winter precipitation (panel b) of the modelled climate values between LGM NHIS 66% and LGM NHIS 100%.

(Kamleitner and others, 2023). The model gives a two-phase LGM advance (Fig. 9) in the right order (the largest is the earliest) and remarkably similar timing ( $\sim 26$  and  $\sim 21$  ka), although the first slightly overshoots the end position (by  $\sim 10$  km, Fig. 8). Furthermore, our model shows another substantial (but less extensive) glaciation of the Reuss Glacier during MIS4, which is in line with the findings of Gaar and others (2019).

#### 3.4.3. Aare Glacier

Aare Glacier was a tributary to the Solothurn lobe of the Rhone Glacier during the LGM climax (see the following section). Our model indicates that both glaciers were connected from 24.5 to 23.1 ka. Wüthrich and others (2018) dated a stabilisation of the Aare Glacier to  $20.7 \pm 2.2$  ka (Gurten stadial). The lack of evidence of a frontal position suggests that the Aare Glacier was still connected to the Rhone Glacier at that time. A frontal

moraine complex in the city of Bern points to a readvance, which Wüthrich and others (2018) dated to  $19.0 \pm 2$  ka. In light of the uncertainties of the dating, the readvance to the Bern stadial position may correspond to the advance seen in the model at 20.5 ka (Figs 9 and 12).

#### 3.4.4. Rhone Glacier, Solothurn lobe

During the LGM, the northern branch of the Rhone Glacier flowed to the north east, forming the Solothurn lobe (Jäckli, 1962; Bini and others, 2009), which merged with the Aare Glacier. Figure 9 shows a single major modelled advance of the Solothurn lobe of the Rhone Glacier with a maximum at 23 ka at a position, which matches the reconstructed lobe of Ehlers and others (2011) (with an undershoot of  $\sim 15$  km, Figs 8 and 12). This result is in good agreement with the cosmogenic  $^{10}\text{Be}$  exposure dating of erratics at Steinhof, which shows that the

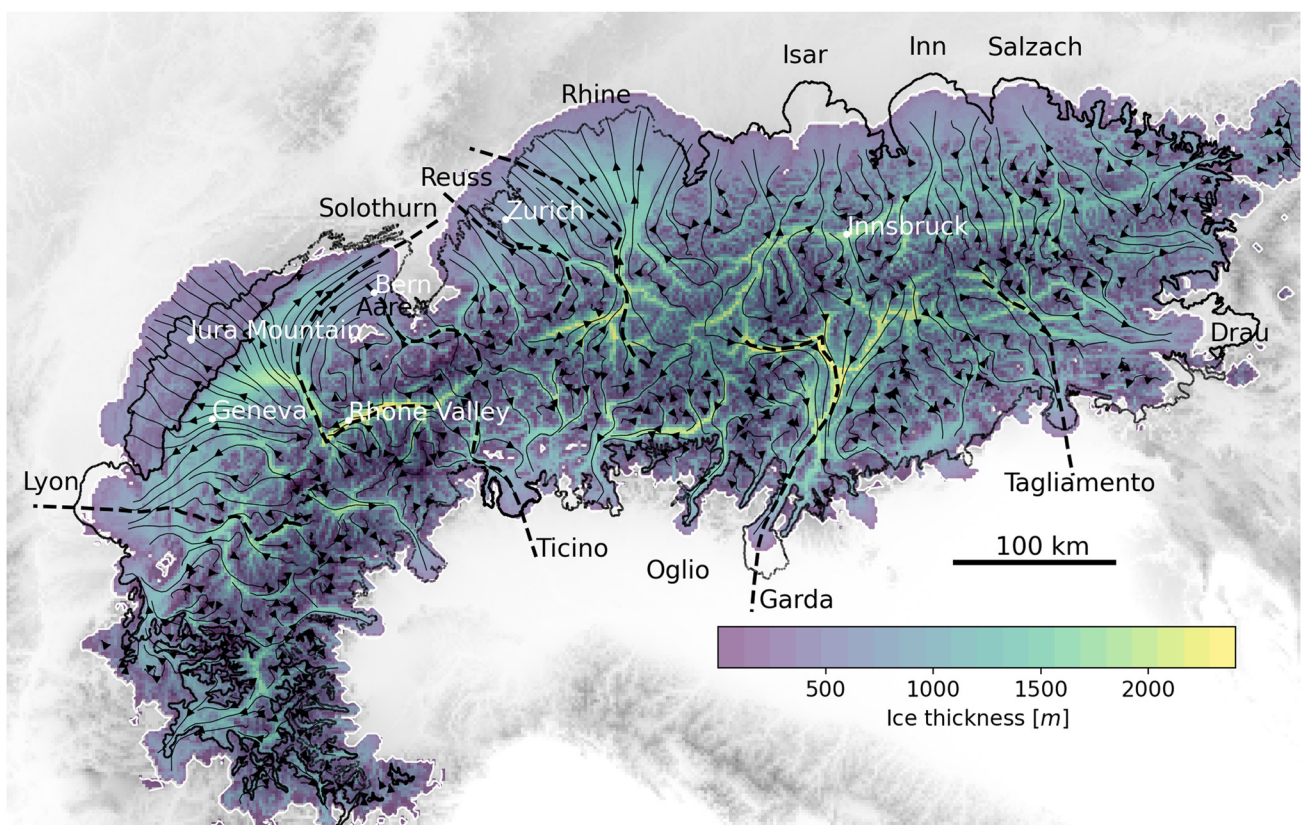


**Figure 8.** Maximum modelled ice thickness and modelled streamlines computed from the surface ice flow at the maximum state (thin lines). For comparison purposes, the reconstructed LGM outline (modified after Ehlers and others (2011)) is shown with a solid line. The dashed lines correspond to flowlines along which the time evolution of individual glaciers is monitored in Figure 9.



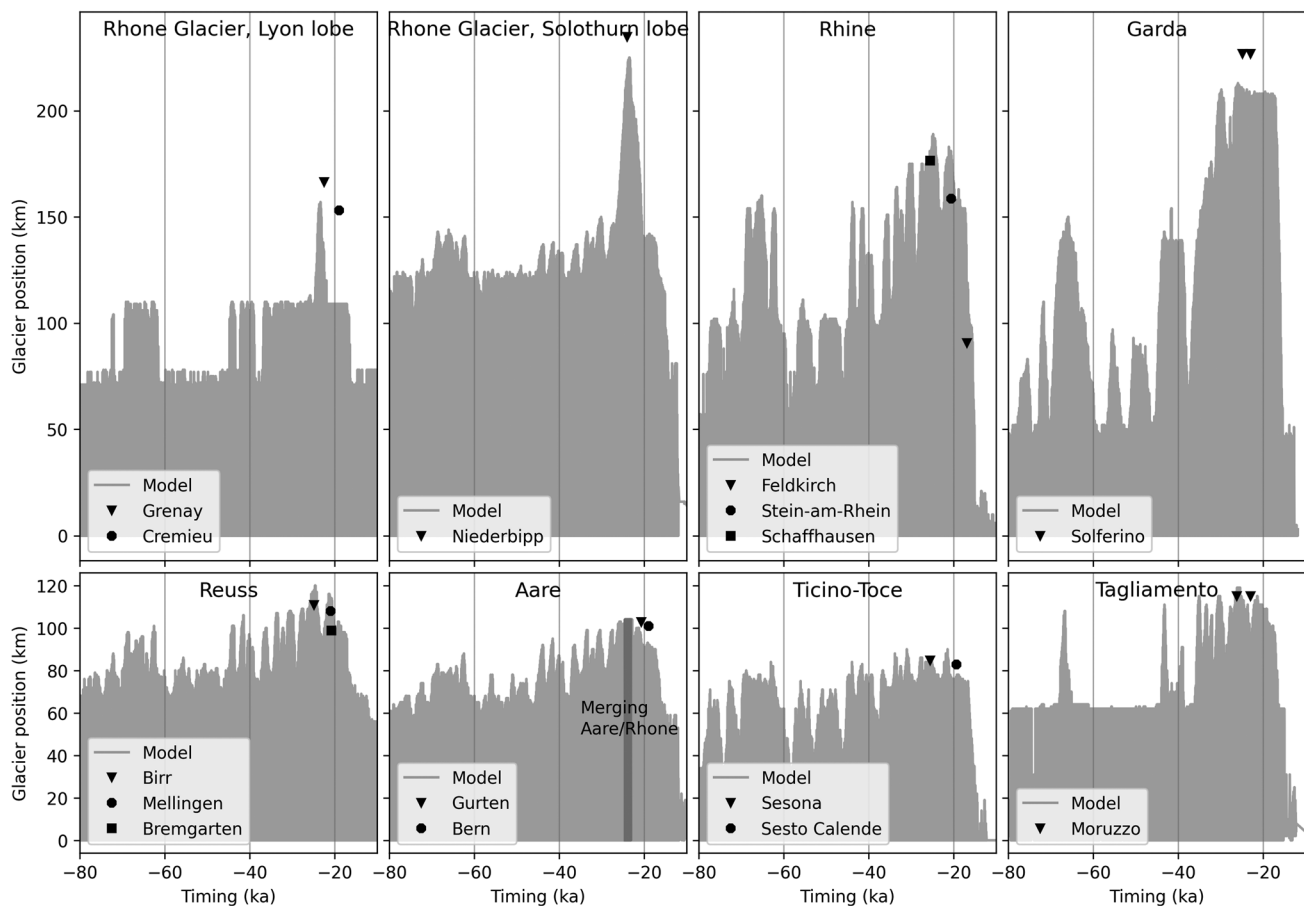


**Figure 9.** Transient advance and retreat of Rhone (Lyon and Solothurn lobes), Rhine, Garda, Reuss, Aare, Ticino-Toce and Tagliamento glaciers from 80 to 10 ka BP along the flowline drawn in Figure 8 compared to field data. Field data from Roattino and others (2023), Ivy-Ochs and others (2004), Kamleitner and others (2023), Monegato and others (2017), Kamleitner and others (2022), Wüthrich and others (2018), Kamleitner and others (2007) and Monegato and others (2007), respectively.

maximum was likely reached at  $24 \pm 2$  ka (Ivy-Ochs and others, 2004; Ivy-Ochs, 2015). In contrast, the modelled Solothurn lobe of the Rhone Glacier is found to have been much smaller during MIS4 (Fig. 11).

### 3.4.5. Jura Mountains

Glacial records in the Jura Mountains, including boulder deposition elevation (Graf and others, 2015), suggest that the mountain range was not covered by ice from the Rhone Glacier, but instead hosted its own ice cap during the LGM (Buoncrisiani and Campy, 2011). This hypothesis is supported by our modelling results. Indeed, our model shows that the climate forcing allows

for such an independent ice cap to form and remain in the Jura Mountains (Fig. 12). The modelled extent, however, exceeds observations in the West. At the LGM, the Jura Mountains with its ice cap constituted a significant obstacle for the ice originating from the Rhone Valley and contributed to split the ice flow coming from the Rhone Valley into two lobes, the Solothurn and Lyon lobes, and prevented the Rhone Glacier from covering the Jura Mountains (Jouviet and others, 2017).

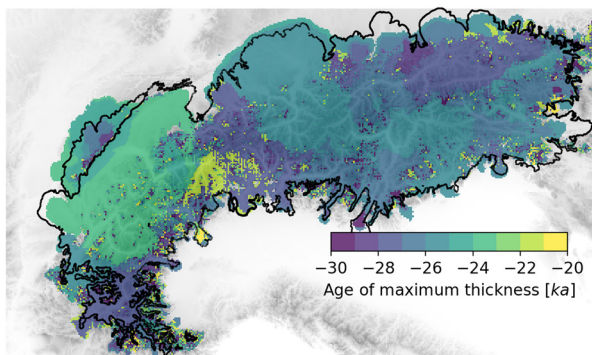


**Figure 10.** Modelled age of maximum ice thickness from 30 to 20 ka BP. The solid line shows the LGM outline modified after Ehlers and others (2011).

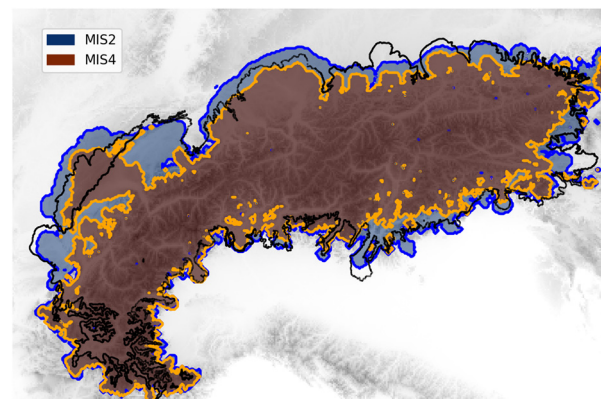


**Figure 11.** Modelled maximum extent during MIS4 compared to the one of MIS2. The solid black line shows the LGM outline modified after Ehlers and others (2011) while the blue and the orange lines show the maximum extent during LGM and MIS4, respectively.

### 3.4.6. Rhone Glacier, Lyon lobe

The modelled LGM extent of the Lyon lobe of the Rhone Glacier shows a single advance with a maximum at about 23.5 ka (Fig. 9), which slightly undershoots the maximum outline from Ehlers and others (2011) (Fig. 8). Therefore, we do not reproduce the two-phase advance scenario suggested by recent surface exposure datings of Roattino and others (2023). Timing of the LGM maximum advance, however, matches field evidence well. The front of the Lyon lobe was found to fluctuate at or close to the LGM maximum position between  $\sim 24$ –21 ka (Roattino and others, 2023). A glacier re-advance was dated to  $19 \pm 1$  ka (Roattino and others, 2023). Furthermore, our simulation supports (stream-lines in Fig. 8) the hypothesis that the Lyon lobe was fed mainly from the French/Savoyan Alps (Coutterand and others, 2009) and not from the Rhone Valley, as evidenced by the absence of boulder lithologies from that region. Lastly, our simulation indicates that LGM was clearly more extensive than MIS4 in this region (Fig. 11), which seems to contradict the two major late Pleistocene glaciations in the western Alpine foreland, during MIS 4 (75–60 ka) and late MIS 3 (40–30 ka) revealed by luminescence dating (Gribenski and others, 2021).

### 3.4.7. South-western Alps

Our model overshoots the maximum outlines documented by Ehlers and others (2011) in the South West Alps. We find several reasons that may explain this discrepancy: (i) the model resolution (2 km) is too poor to resolve the complex topography of this region and the relatively small glacier catchments, (ii) the climate model overestimates precipitation in this region, as evident from a comparison against available pollen-based reconstructions (Davis and others, 2022; Russo and others, 2022), (iii) the outlines given by Ehlers and others (2011) correspond to a more recent maximum than the LGM, which occurred around 24 ka in the Maritime Alps, as shown by exposure dates from the Stura and Gesso valleys Ribolini and others (2022). Note that Višnjević

and others (2020) have already evidenced that the outlines of this region correspond to very high ELAs in comparison to the rest of the Alps, questioning the timing of these outlines.

### 3.4.8. Ticino-Toce, Oglio, Garda and Tagliamento lobes

Analysis and dating of moraines have revealed incredibly synchronous LGM maxima of Southern Alpine glacier systems. The Dora Riparia Glacier reached its LGM maximum extent in the Rivoli-Avigliana end moraine system at  $24.0 \pm 1.5$  ka (Ivy-Ochs and others, 2018). A major glacier re-advance was reconstructed at  $19.6 \pm 0.9$  ka (Ivy-Ochs and others, 2018). The Ticino-Toce Glacier fluctuated at or close to its LGM maximum position from ca.  $25 \pm 1$  ka to ca.  $20 \text{ ka} \pm 1 \text{ ka}$  (Kamleitner and others, 2022). A late LGM readvance was dated  $19.7 \pm 1.1$  ka (Kamleitner and others, 2022) and  $19 \pm 1$  ka (Braakhekke and others, 2020), in Verbano and Orta lobes, respectively. Reaching of the LGM maximum extent in the Oglio Glacier system was constrained to 26.4–25.3 ka cal BP (Ravazzi and others, 2012). A two-phased LGM maximum at 25.0–24.2 and 23.3–23.1 ka cal BP was found for the Garda lobe (Adige-Sarca Glacier, Monegato and others, 2017). Tagliamento glacier reached its biggest extent at 28.0–24.5 ka cal BP, with a re-advance to nearly the same position at 23.2–22.8 ka cal BP (Monegato and others, 2007). Furthermore, the aforementioned studies evidenced the collapse and clear-up of the valley floors relatively quickly after the last re-advance, namely between 19 and 17.2 ka.

Figure 9 shows the evolution of three of the four lobes and compares them with the space-time positions of the glacier margin documented by Kamleitner and others (2022) and Monegato and others (2017, 2007). Our model shows a good fit for the Tagliamento and the Ticino-Toce lobes (Fig. 8), but the Garda Glacier is too small (by  $\sim 15$  km). The two-phase advance of the Tagliamento Glacier is generally well captured; however, the timings of these two events differ slightly (within the uncertainty range) from those documented. In contrast, the Garda lobe is

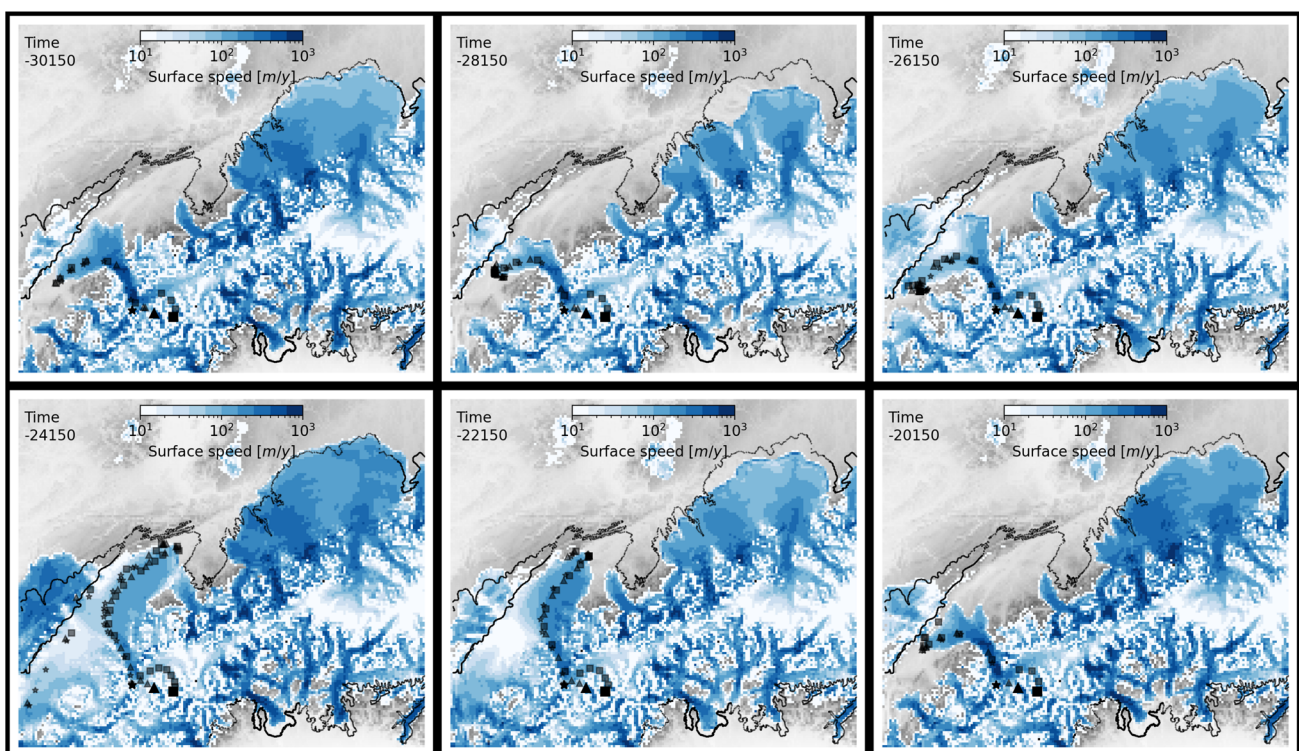


**Figure 12.** Transient evolution of the Central Alpine glacier systems around the LGM. The magnitude of the surface ice speed and the trajectory of erratic boulders from Valais are shown. The symbols  $\star$ ,  $\blacktriangle$  and  $\blacksquare$  represent markers seeded at Mont Blanc, Val de Bagnes and Val d'Arolla, respectively. The solid line shows the LGM outline modified after Ehlers and others (2011).

found to be fairly stable close to LGM. Lastly, the rapid collapse of the lobes is in general well reproduced by the model; however, it occurs  $\sim 15$  ka, i.e. a few millennia after the timing given in the references.

### 3.4.9. Eastern Alps

Although the easternmost Alps have well-mapped maximum ice margins (Van Husen, 1987; Ehlers and Gibbard, 2008) there exist very little quantitative age constraints to reconstruct the spatio-temporal evolution of glaciers in this region of the Alps (Wölfler and others, 2021). With the exception of the southern lobe (Drau Glacier, Schmidt and others, 2012), whose extent is underestimated (by  $\sim 40$  km), our modelled maximum ice extent reproduces the mapped ice margins well (Fig. 8).

### 3.4.10. Salzach, Inn and Isar lobes

In the north east of the Alps, the model roughly reproduces the Salzach lobe, underestimates the Inn lobe, and largely underestimates the Isar lobe (by  $\sim 40$  km) as mapped by Van Husen (1987) (compiled by Ehlers and Gibbard, 2008). This suggests that our modelled LGM climate may have underestimated precipitation or overestimated temperature in the catchment of the Inn and Isar lobes. In addition, the model shows uniform glacier extents on the northern foreland, while the geological reconstruction shows three well-distinct lobes. This may be due to the fact that the basal topography used in the model (the present-day surface topography) includes sediment layers that may have been absent at the LGM. Lastly, our model indicates that the maximum was reached at  $\sim 26$  ka BP (Fig. 10).

## 3.5. Ice thickness and flow pattern around the Rhone catchment

The Rhone Glacier basin contains several well-documented geomorphological findings related to the last glaciation that allow us to assess our modelling results in terms of ice flow patterns and ice thickness. We now describe in turn the compatibility of our model results with erratic boulders, trimlines and erosional features of transfluences.

First, by integrating the modelled transient ice flow velocities, we reconstruct the transport and deposition of erratic boulders. Figure 12 shows the modelled trajectories of boulders originating from the southern Rhone Valley and Mont Blanc as in Jouvét and others (2017). The results show that a large number of these modelled erratic boulders are deposited in the Solothurn lobe during the retreating stage (Fig. 12, bottom panels), consistent with the lithology characteristics of the boulders found in this region (e.g. Burkard and Spring, 2004; Graf and others, 2015).

Second, trimlines in the Alps were mostly interpreted as a marker of the maximum elevation of the ice surface (e.g. Florineth and Schlüchter, 2000; Kelly and others, 2004; Bini and others, 2009) and therefore should coincide with the maximum vertical extent of our model. However, comparing the maximum modelled ice thickness to the trimlines of the Rhone Valley documented by Kelly and others (2004) reveals a bias: the modelled maximum ice surface is overestimated by  $\sim 387$  m on average (Fig. 13), which is approximately 50% of the ice thickness in this region. This bias may be the result of simplification (SIA) in the PISM iceflow model (Imhof and others, 2019) and too poor spatial resolution: 2 km does not resolve the complex topography of high mountain summits and cannot represent the steep ridges on which trimlines are observed. As a result, the ice accumulates over the highest model grid cells without being evacuated due to cold-based slow motion and gentle slopes caused by averaging. This in turn may cause the ice thickness to be overestimated in the highest regions. The hypothesis that the timelines reflect the warm-

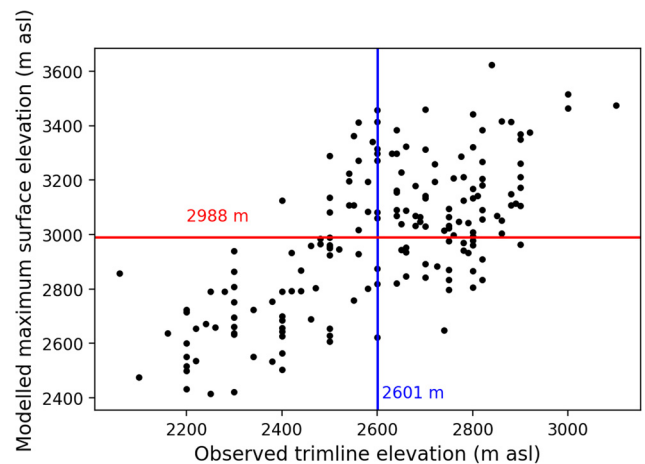


**Figure 13.** Modelled maximum ice surface (corrected for the depression of the bedrock) versus observed trimline elevations in the Rhone Valley by Kelly and others (2004) (Fig. 14). The modelled ice thickness is overestimated by 387 m on average compared to trimlines.

cold base transition rather than the maximum surface elevation is another reason that may explain the discrepancy (Cohen and others, 2018; Seguinot and others, 2018).

Finally, despite an overestimation of the ice thickness, our simulation depicts the AIF as a network of glaciers whose flow is mainly controlled by the basal topography. The modelled ice flow field at the border of the Rhone catchment shows clear transfluences (Fig. 14). This includes the southward transfluence across the Simplon Pass into the Toce Glacier catchment and the transfluence across Brünig Pass from the Aare catchment (right tributary of the Rhone glacier) to the Reuss glacier system (Jäckli, 1962; Kelly and others, 2004; Bini and others, 2009).

## 3.6. Sensitivity to model parameters

In this section, we present the results of three additional model runs to assess the influence of important parameters on our model results.

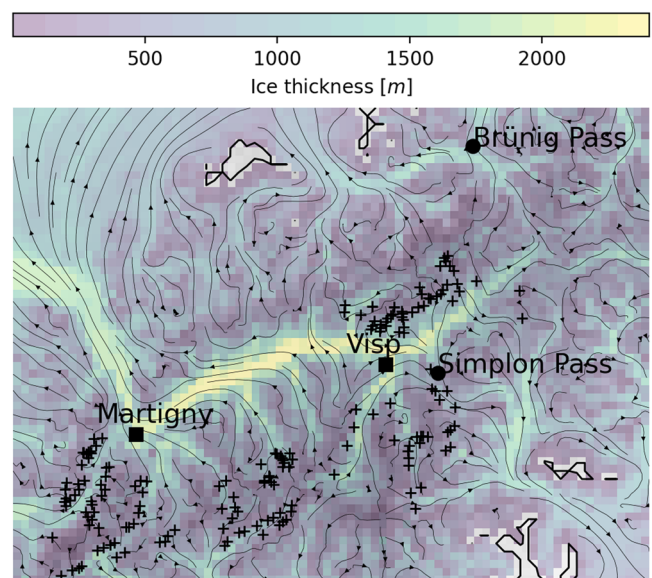


**Figure 14.** Modelled maximum ice thickness in the Rhone catchment. Continuous lines indicate the streamlines computed from the surface ice flow at the maximum state. The two transfluences (Simplon and Brünig) are shown with black dots. The black crosses correspond to places where trimlines have been documented in the Rhone Valley by Kelly and others (2004).

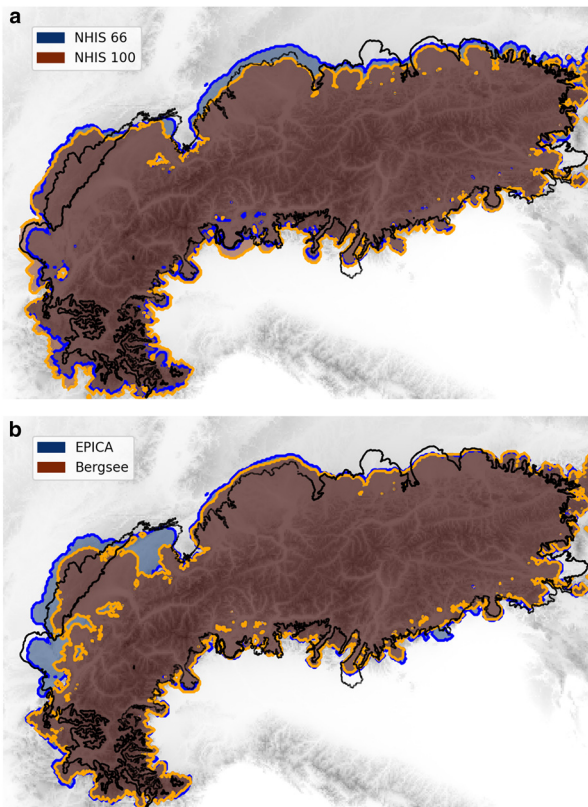


**Figure 15.** Modelled maximum extent during LGM using NHIS 100% (panel a) and Bergsee signal (panel b) compared to the reference simulation that uses 66% NHIS and EPICA. The solid black line shows the reconstructed LGM outline modified after Ehlers and others (2011), the blue shows the reference simulation while the orange line shows the NHIS 100% (panel a) and Bergsee signal (panel b) simulations, respectively.

### 3.6.1. Influence of the size of the NHIS

We model the AIF during the last glacial cycle using climate forcing based on the assumption of 100% NHIS (instead of 66%) to measure the influence of this parameter. To maintain a similar ice extent at the LGM, the melting parameter is tuned to  $C = 0.9$  (Fig. 15, top panel). There are, however, notable local discrepancies between glacier lobes: the 100% NHIS climate forcing produces more extensive glaciers in the south with some notable overshoots (e.g. Ticino-Toce), and less extensive glaciers in the north resulting in several good matches (e.g. Solothurn and Rhine lobes), and some undershoots (e.g. lobes in the northeast). This result is in line with the difference between the precipitation patterns of the two forcings (Fig. 7).

### 3.6.2. Influence of the climate signal

We have performed simulations with different climate signals including EPICA (Jouzel and others, 2007), NGRIP (Seierstad and others, 2014) and the local pollen-based signal from Bergsee, Southern Germany (Duprat-Qualid and others, 2017), which correlates relatively well with NGRIP in terms of variability, to drive the glacial index transient climate. An important difference between the EPICA and Bergsee signals is that the glacial index prior to the LGM is generally smaller, i.e. the length of the time period with a GI close to one is shorter (Fig. 3) for the Bergsee signal. As a result, we notice in general very minor or no differences with the EPICA simulation except for the Rhone Glacier, which is largely underestimated (Fig. 15, bottom panel). This experiment shows that the considerable size of the Rhone Glacier at LGM is the result of prolonged cold conditions in the climate forcing, and that the duration these conditions prevail is an essential parameter that must be considered to model

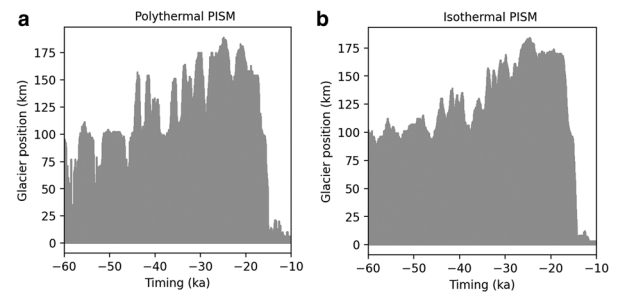


**Figure 16.** Transient advance and retreat of the Rhine Glacier (as in Fig. 9) using a polythermal model (panel a), and using an isothermal model (switching off the ice temperature, panel b).

the transient evolution of the AIF in agreement with the known LGM glacier footprints. This additional sensitivity experiment highlights the dependence to the chosen climate signal, and the limitation of our GI approach to reproduce glacier states different from LGM in the absence of tuning data.

### 3.6.3. Importance of modelling the ice thermo-mechanics

In a last sensitivity model experiment, we run the isothermal version of PISM by switching off the thermal component of the model. Figure 16 compares the fluctuations of the Rhine Glacier using these two settings: (i) the polythermal reference version discussed in this paper and (ii) the isothermal version. The polythermal model shows many more fluctuations than the isothermal model, indicating that the amplification of glacier fluctuations is the direct consequence of feedback mechanisms in the thermo-mechanics of ice. When glacier ice temperature is modelled, cooling causes successively a thick glacier lobe to form, temperate basal conditions to occur due to thermal isolation, downwasting of ice due to enhanced sliding and evacuation of ice to the ablation zone leading to glacier retreat. In contrast, the AIF clearly shows much fewer fluctuations (only long-term climate-induced ones) when switching off the thermal component of the model. In summary, this model experiment shows that the frequent glacier oscillations displayed by the model are partly non-climatic as the EPICA climate signal chosen to drive the glacial index is relatively smooth (Fig. 3). In fact, they are the consequence of positive feedback mechanisms between the basal ice temperature, the basal sliding and the ice thickness. This shows that while climate is the main driver that leads to major glaciations, non-climatic internal glacier thermomechanics may play an equally important role in explaining the dynamical behaviour of glaciers.

### 3.7. Importance of climate modelling

The benefit of modelling the climate of glacial states can be illustrated by comparing our simulation at the LGM to the one of Seguinot and others (2018), who used the same ice-flow model (at 1 km) but with a paleoclimate based on a distortion of today's climate driven by the EPICA signal. While there exist important discrepancies (100 km eastward shift) between the LGM ice margin mapped from geomorphological evidence and the one predicted by Seguinot and others (2018), our new model (and independently of the assumption on the NHIS height) mostly resolves this discrepancy (Fig. 17), especially in the Western lobes (Lyon and Solothurn) and in the eastern Alps. This result shows that the modelled precipitation pattern, which features notably more precipitation in the western Alps at the LGM (Fig. 5), is a key factor to reproduce the AIF ice cover consistent with moraine-based reconstructions. As a corollary, our results demonstrate the importance of the shift of the westerlies in the building-up of the AIF (Fig. 1).

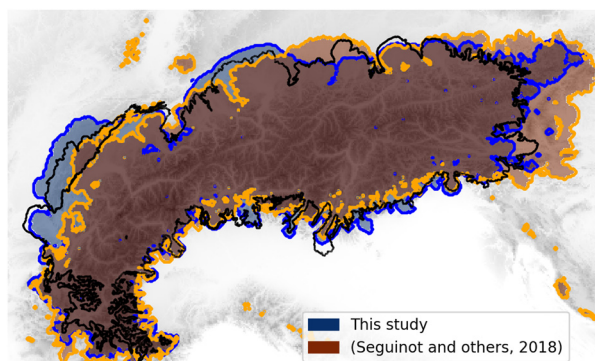


**Figure 17.** Comparison of the maximum ice extent modelled by Seguinot and others (2018) and in the present study. The solid black line shows the reconstructed LGM outline modified after Ehlers and others (2011), the blue shows our reference simulation while the orange line shows the one of Seguinot and others (2018).

Another important difference between modelled and geological evidence is the ice thickness in the Rhone Valley: our simulation overestimates the ice thickness by 387 m on average using trimlines as reference of the maximum elevation of the ice surface (Fig. 13). This is about 60% less than the ice thickness overestimate of Seguinot and others (2018). The difference between the two models is presumably due to temperature differences in the climate forcing: our forcing causes smaller cold basal areas. This, in turn, increases basal motion and ice fluxes and thus contributes to thinning the ice at high elevations. The modelled climate forcing used in this study, therefore, contributes to reducing the mismatch between the modelled maximum surface elevation and the trimlines. The remaining discrepancy, which is still significant, is mainly attributed to the horizontal resolution of the model (2 km), which cannot capture complex three-dimensional topography, and possibly to simplification in modelled ice physics (Imhof and others, 2019). Despite the thinner AIF, the model reproduces two major transfluences at the Simplon and Brünning passes well (Fig. 14).

Tracking the trajectory of erratic boulders in the Solothurn lobe near the LGM is important for evaluating the model against field evidence (Jouvét and others, 2017). Indeed, many erratics with lithologies characteristic of southern Valais and Mont Blanc were found in the northern Solothurn lobe (e.g. Burkard and Spring, 2004; Graf and others, 2015; Jouvét and others, 2017), demonstrating that the boulders must have been diverted across the centreline of the Rhone Valley (Kelly and others, 2004) during the LGM. Previous modelling studies showed that this boulder diversion is highly conditioned to the distribution of precipitation in the Alps (Jouvét and others, 2017) or transient effects on climate forcing (Imhof, 2021). In our simulation, the modelled erratic boulders from the southern Valais are first transported towards Geneva during the first advance phase when the Solothurn lobe is relatively small (Fig. 12, top panels). Then, when the Solothurn lobe grows until it reaches its maximum, a clear switch from east-south to northwest occurs in the dominant ice flow direction causing boulders to be diverted (Fig. 12, bottom panels). The diversion, which is maintained during the entire deglaciation of the Rhone Glacier, is consistent with today's distribution of erratic boulders.

### 3.8. Importance of transient glacier modelling

Beside climate modelling, our results also illustrate the importance of using a physical and time evolving glacier model to reproduce the AIF dynamics and its transient behaviour:

- Modelling the climate and the resulting glacier response in a transient way is essential to capture glacier volumes and inertia

(Fig. 15, bottom panel), glacier fluctuations (Fig. 16) and the timing of maxima (Fig. 9).

- Accounting for the ice dynamics is essential to reproduce the ice flow pattern revealed by erratic boulders or erosional features, as well as the inertia of glaciers of various sizes and the resulting timing of maxima (Fig. 12).
- Modelling the thermomechanics of ice and the feedback between basal conditions and climate forcing is important to reproduce glacier fluctuations revealed by moraine mapping and dating (Figs 9 and 16).

These results justify our choice of using a multiphysics model such as PISM, but also highlight the limitations of simpler models (e.g. Del Gobbo and others, 2023) that do not consider ice dynamics or transient glacier evolution, and thus cannot capture these features.

## 4. Conclusions

In this work, we have simulated the climatic conditions and the resulting glacier evolution in the European Alps over the last glacial cycle at a high spatial resolution (2 km) by coupling for the first time a climate model to an ice-flow model. Only minor adjustments of the melting parameters (on the order of 10%) were needed to model the AIF consistently with geomorphological reconstructions demonstrating the coherence of both the climate and glacier models. Our study allows us to simultaneously overcome shortcomings of previous studies in terms of paleoclimate forcing (Seguinot and others, 2018) and glacier modelling (Višnjević and others, 2020; Del Gobbo and others, 2023). Comparisons with field evidence in terms of maximum horizontal and vertical glacier extents, as well as in terms of ice dynamics, show that the model reproduces LGM-related field observations: (1) the moraine-based maximum extents are well reproduced with only minor regional exceptions; (2) the trajectory of erratic boulders in the Rhone Valley is consistent with observations at the Solothurn lobe; (3) the trimline-based vertical maximum ice surface elevation in the Rhone Valley is reproduced with a limited bias leading to a moderate overestimation of the ice thickness; (4) two transfluences from the Rhone/Aare catchment documented by glacial erosion features are well reproduced by the model. Our results remain limited by uncertainties in climate and glacier modelling and spatial resolution. Indeed, the EPICA signal together with the climate states is not meant to represent the full timing and complexity of the last glacial paleoclimate in the Alps revealed by proxy records (e.g. Duprat-Oualid and others, 2017; Luetscher and others, 2015), but is used to build the AIF consistently with geomorphological evidence during glacial maxima. Therefore, our modelled results related to intermediate states and the Holocene must be interpreted with caution. Furthermore, the 2 km model grid cell is too coarse to model small-scale glaciers during the Holocene and capture complex glacial reliefs through the entire simulation period. This probably partly explains the overestimation of the ice thickness.

Difficulties to constrain different model parameters may affect our modelling results: for instance, we found that climate modelling results are sensitive to the assumption on the height of the NHIS. We tuned the mass-balance melt parameters to match the LGM glacier extent, as they are among the least constrained parameters (and are expected to vary spatially to account for different sources of melt). Another tuning strategy (e.g. through climate GI variables) with different mass-balance parameters could modify the glacier response to climate, especially between small and large lobes. Examples of model parameters that exert a first-order control of the ice flow, and therefore may influence the dynamic response of the AIF to climate forcing are the till friction

angle in the Mohr–Coulomb sliding law and parameters of the subglacial hydrology model.

Similarly to Del Gobbo and others (2023), our climate model results demonstrate the importance of climate to force paleo glacier models to reproduce the precipitation pattern and ice geometry consistent with the geomorphologically reconstructed distribution of LGM glaciers in the Alps. The LGM precipitation pattern is found to be different from that prevailing in modern times (Fig. 5) probably due to significant changes in global atmospheric circulation between glacial and interglacial periods (Fig. 1). Our results show that a consistent precipitation pattern is necessary but not sufficient to reproduce key observed features. Including both transient climate and the thermomechanics of glacier evolution were found equally important to capture the ice flow patterns as well as the spatiotemporal fluctuations of glaciers, which strongly vary according to the size of glacier basins. In that perspective, key aspects to be improved are the modelling of a truly transient climate to better represent the entire glacial cycle, overcome the shortcomings of the GI approach and reduce the uncertainty due to the choice of the climate signal. Transient high-resolution downscaling of temperature and precipitation data during deglaciation (from LGM to the Holocene) proposed by Karger and others (2023) is a promising approach to address this issue.

Achieving subkilometre spatial resolution is another essential aspect that must be investigated in future work to resolve ice fluxes in the rugged topography of the Alps and the resulting ice thickness, which remain subject to biases between geomorphological and modelled-based reconstructions. We also noticed that high resolution is crucial for handling interglacial states such as during the Holocene. Unfortunately, modelling the entire Alps at subkilometre spatial resolution is prohibitively expensive with physical traditional glacier models. In that perspective, a new modelling approach (Jouvet and Cordonnier, 2023) based on deep learning emulation and Graphical Processing Units offers a promising perspective to overcome the computational bottleneck and achieve a spatial resolution that is suitable for describing the complex topography of the Alpine mountains.

**Data.** The glacier evolution modelling results are freely available at <https://doi.org/10.5281/zenodo.8270674>.

**Acknowledgements.** This research was funded by the National Cooperative for the Disposal of Radioactive Waste (NAGRA), and the Swiss National Science Foundation (SNSF, project 200021–162444). Climate simulations were performed on the supercomputing architecture of the Swiss National Supercomputing Centre (CSCS). Guillaume Jouvet thank Andreas Vieli and Martin Funk for their support and inspiring discussions, the PISM developing team (Constantine Khroulev, Andy Aschwanden, Ed Bueler) for support, Natacha Gribenski for inspiring Figure 1, Fanny Duprat Oualid and Damien Rius for giving access to the data of the Bergsee signal.

**Author contributions.** The ice flow modelling was performed by Guillaume Jouvet with the help of Denis Cohen. The climate modelling was performed by Emmanuele Russo, Jonathan Buzan and Christoph Raible. Guillaume Jouvet analysed the glacier modelling results with support from Sarah Kamleitner and Susan Ivy-Ochs for comparison with geomorphological and dating evidence. Guillaume Jouvet wrote the paper with inputs from all coauthors. The research of this paper was conceived as part of EIDER project led by Guillaume Jouvet, Denis Cohen, Urs Fischer and Angela Landgraf.

## References

- Antoine P and 7 others (2009) Rapid and cyclic aeolian deposition during the Last Glacial in European loess: a high-resolution record from Nussloch, Germany. *Quaternary Science Reviews* **28**(25–26), 2955–2973. doi:10.1016/j.quascirev.2009.08.001
- Aschwanden A, Bueler E, Khroulev C and Blatter H (2012) An enthalpy formulation for glaciers and ice sheets. *Journal of Glaciology* **58**(209), 441–457. doi:10.3189/2012JG11J088
- Balco G (2011) Contributions and unrealized potential contributions of cosmogenic-nuclide exposure dating to glacier chronology, 1990–2010. *Quaternary Science Reviews* **30**(1–2), 3–27. doi:10.1016/j.quascirev.2010.11.003
- Ban N, Schmidli J and Schär C (2014) Evaluation of the convection-resolving regional climate modeling approach in decade-long simulations. *Journal of Geophysical Research: Atmospheres* **119**(13), 7889–7907. doi:10.1002/2014JD021478
- Bartlein PJ and 18 others (2011) Pollen-based continental climate reconstructions at 6 and 21 ka: a global synthesis. *Climate Dynamics* **37**(3–4), 775–802. doi:10.1007/s00382-010-0904-1
- Batchelor CL and 8 others (2019) The configuration of northern hemisphere ice sheets through the Quaternary. *Nature Communications* **10**(1), 3713. doi:10.1038/s41467-019-11601-2
- Bini A and 10 others (2009) Die Schweiz während des letzteiszeitlichen maximums (LGM), Karte 1:500 000 [Map]. Bundesamt für Landestopografie swisstopo.
- Braakhekke J and 6 others (2020) Timing and flow pattern of the Orta glacier (European Alps) during the Last Glacial Maximum. *Boreas* **49**(2), 315–332. doi:10.1111/bor.12427
- Braithwaite RJ (1995) Positive degree-day factors for ablation on the Greenland ice sheet studied by energy-balance modeling. *Journal of Glaciology* **41**(137), 153–160. doi:10.3189/S0022143000017846
- Braithwaite RJ and Zhang Y (2000) Sensitivity of mass balance of five Swiss glaciers to temperature changes assessed by tuning a degree-day model. *Journal of Glaciology* **46**(152), 7–14. doi:10.3189/172756500781833511
- Bueler E and Brown J (2009) Shallow shelf approximation as a ‘sliding law’ in a thermomechanically coupled ice sheet model. *Journal of Geophysical Research – Earth Surface* **114**(F3), 1–21. doi:10.1029/2008JF001179
- Bueler E, Lingle CS and Kallen-Brown J (2007) Fast computation of a viscoelastic deformable earth model for ice sheet simulation. *Annals of Glaciology* **46**, 97–105. doi:10.3189/172756407782871567
- Buoncrisiani JF and Campy M (2011) Quaternary glaciations in the French Alps and Jura. In Ehlers J, Gibbard PL and Hughes PD (eds), *Quaternary Glaciations – Extent and Chronology – A Closer Look*, volume 15 of *Developments in Quaternary Sciences*. Amsterdam: Elsevier, pp. 117–126. doi:10.1016/b978-0-444-53447-7.00010-6
- Burkard M and Spring J (2004) Erratic boulders of the ancient Rhone glacier and the dispersal pattern of Mt. Blanc granites. In *2nd Swiss Geoscience Meeting*, Lausanne, pp. 102–103.
- Buzan JR, Russo E, Kim WM and Raible CC (2023) Winter sensitivity of glacial states to orbits and ice sheet heights in CESM1.2. *EGU Sphere* **2023**, 1–30. doi:10.5194/egusphere-2023-324
- Calov R and Greve R (2005) Correspondence: a semi-analytical solution for the positive degree-day model with stochastic temperature variations. *Journal of Glaciology* **51**(172), 173–175. doi:10.3189/172756505781829601
- Cleator SF, Harrison SP, Nichols NK, Prentice IC and Roulstone I (2020) A method for generating coherent spatially explicit maps of seasonal paleoclimates from site-based reconstructions. *Journal of Advances in Modeling Earth Systems* **12**(1), 1–15. doi:10.1029/2019MS001630
- Cohen D, Gillet-Chaulet F, Haerberli W, Machguth H and Fischer UH (2018) Numerical reconstructions of the flow and basal conditions of the Rhine glacier, European Central Alps, at the Last Glacial Maximum. *The Cryosphere* **12**(8), 2515–2544. doi:10.5194/tc-12-2515-2018
- Coutterand S, Schoeneich P and Nicoud G (2009) Le lobe glaciaire lyonnais au maximum würmien: glacier du Rhône ou/et glaciers savoyard? Collection EDYTEM- Cahiers de Géographie, n°8, pp. 11–22.
- Cuffey K and Paterson W (2010) *The physics of glaciers*. Academic Press.
- Davis B, Fasel M, Kaplan J, Russo E and Burke A (2022) The climate and vegetation of Europe, North Africa and the Middle East during the Last Glacial Maximum (21 000 years BP) based on pollen data. *Climate of the Past Discussions* 1–66. doi:10.5194/cp-2022-59
- Del Gobbo C, Colucci RR, Monegato G, Žebre M and Giorgi F (2023) Atmosphere-cryosphere interactions during the last phase of the Last Glacial Maximum (21 ka) in the European Alps. *Climate of the Past* **19**, 1805–1823. doi:10.5194/cp-19-1805-2023
- Dong B and Valdes P (1998) Simulations of the Last Glacial Maximum climates using a general circulation model: prescribed versus computed sea surface temperatures. *Climate Dynamics* **14**(7–8), 571–591. doi:10.1007/s003820050242
- Duprat-Oualid F and 6 others (2017) Vegetation response to abrupt climate changes in Western Europe from 45 to 14.7 k cal a BP: the Bergsee

- lacustrine record (Black Forest, Germany). *Journal of Quaternary Science* 32(7), 1008–1021. doi:10.1002/jqs.2972
- Ehlers J and Gibbard P** (2008) Extent and chronology of Quaternary glaciation. *Episodes* 31(2), 211–218.
- Ehlers J, Gibbard PL and Hughes PD** (2011) *Quaternary Glaciations - Extent and Chronology — A Closer Look*, volume 15 of *Developments in Quaternary Science*. Amsterdam: Elsevier.
- Fallah B, Sodoudi S and Cubasch U** (2016) Westerly jet stream and past millennium climate change in arid central Asia simulated by COSMO-CLM model. *Theoretical and Applied Climatology* 124(3), 1079–1088. doi:10.1007/s00704-015-1479-x
- Fallah B and 5 others** (2018) Towards high-resolution climate reconstruction using an off-line data assimilation and COSMO-CLM 5.00 model. *Climate of the Past* 14(9), 1345–1360. doi:10.5194/cp-14-1345-2018
- Farinotti D and 6 others** (2019) A consensus estimate for the ice thickness distribution of all glaciers on earth. *Nature Geoscience* 12(3), 168–173. doi:10.1038/s41561-019-0300-3
- Florineth D and Schlüchter C** (2000) Alpine evidence for atmospheric circulation patterns in Europe during the LGM. *Quaternary Research* 54(3), 295–308. doi:10.1006/qres.2000.2169
- Gaar D, Graf HR and Preusser F** (2019) New chronological constraints on the timing of Late Pleistocene glacier advances in northern Switzerland. *E&G Quaternary Science Journal* 68(1), 53–73. doi:10.5194/egqsj-68-53-2019
- Gosse JC and Phillips FM** (2001) Terrestrial in situ cosmogenic nuclides: theory and application. *Quaternary Science Reviews* 20(14), 1475–1560. doi:10.1016/S0277-3791(00)00171-2
- Goutorbe B, Poort J, Lucazeau F and Raillard S** (2011) Global heat flow trends resolved from multiple geological and geophysical proxies. *Geophysical Journal International* 187, 1405–1419. doi:10.1111/j.1365-246X.2011.05228.x
- Graf A and 8 others** (2015) Multiple advances of Alpine glaciers into the Jura Mountains in the Northwestern Switzerland. *Swiss Journal of Geosciences* 108, 225–238. doi:10.1007/s00015-015-0195-y
- Gribenski N and 5 others** (2021) Out-of-phase Late Pleistocene glacial maxima in the Western Alps reflect past changes in North Atlantic atmospheric circulation. *Geology* 49(9), 1096–1101. doi:10.1130/G48688.1
- Heyman BM, Heyman J, Fickert T and Harbor JM** (2013) Paleo-climate of the central European uplands during the Last Glacial Maximum based on glacier mass-balance modeling. *Quaternary Research* 79(1), 49–54. doi:10.1016/j.yqres.2012.09.005
- Hock R** (2003) Temperature index melt modelling in mountain areas. *Journal of Hydrology* 282, 104–115. doi:10.1016/S0022-1694(03)00257-9
- Hofer D, Raible CC, Dehnert A and Kuhlemann J** (2012a) The impact of different glacial boundary conditions on atmospheric dynamics and precipitation in the North Atlantic region. *Climate of the Past* 8, 935–949. doi:10.5194/cp-8-935-2012
- Hofer D, Raible CC, Dehnert A and Kuhlemann J** (2012b) Simulated winter circulation types in the North Atlantic and European region for pre-industrial and glacial conditions. *Geophysical Research Letters* 39(15), 15805. doi:10.1029/2012GL052296
- Hurrell JW and 22 others** (2013) The community earth system model: a framework for collaborative research. *Bulletin of the American Meteorological Society* 94(9), 1339–1360. doi:10.1175/BAMS-D-12-00121.1
- Imhof MA** (2021) *Combined climate-ice flow modelling of the Alpine ice field during the Last Glacial Maximum*. Ph.D. thesis, ETH Zurich.
- Imhof MA and 5 others** (2019) Modelling a paleo valley glacier network using a hybrid model: an assessment with a Stokes ice flow model. *Journal of Glaciology* 65(254), 1000–1010. doi:10.1017/jog.2019.77
- Ivy-Ochs S** (2015) Glacier variations in the European Alps at the end of the last glaciation. *Cuadernos de investigación geográfica* 41(41), 295–315. doi:10.18172/cig.2750
- Ivy-Ochs S and Kober F** (2008) Surface exposure dating with cosmogenic nuclides. *E&G Quaternary Science Journal* 57(12), 179–209. doi:10.3285/eg.57.1-2.7
- Ivy-Ochs S, Schäfer J, Kubik PW, Synal HA and Schlüchter C** (2004) Timing of deglaciation on the Northern alpine foreland (Switzerland). *Eclogae Geologicae Helveticae* 97(1), 47–55. doi:10.1007/s00015-004-1110-0
- Ivy-Ochs S and 9 others** (2018) New geomorphological and chronological constraints for glacial deposits in the Rivoili-Avigliana end-moraine system and the lower Susa Valley (Western Alps, NW Italy). *Journal of Quaternary Science* 33(5), 550–562. doi:10.1002/jqs.3034
- Ivy-Ochs S, Monegato G and Reitner JM** (2022) The Alps: glacial landforms from the Last Glacial Maximum. In *European Glacial Landscapes*, Elsevier, pp. 449–460.
- Jäckli H** (1962) Die Vergletscherung der Schweiz im Würm maximum. *Eclogae Geologicae Helveticae* 55, 285–295.
- Juvet G and Cordonnier G** (2023) Ice flow model emulator based on physics-informed deep learning. *Journal of Glaciology* in press.
- Juvet G, Seguinot J, Ivy-Ochs S and Funk M** (2017) Modelling the diversion of erratic boulders by the Valais Glacier during the Last Glacial Maximum. *Journal of Glaciology* 63(239), 487–498. doi:10.1017/jog.2017.7
- Jouzel J and 9 others** (2007) Orbital and millennial Antarctic climate variability over the past 800 000 years. *Science* 317(5839), 793–796. doi:10.1126/science.1141038
- Kageyama M, Valdes P, Ramstein G, Hewitt C and Wyputta U** (1999) Northern hemisphere storm tracks in present day and Last Glacial Maximum climate simulations: a comparison of the European PMIP models. *Journal of Climate* 12(3), 742–760. doi:10.1175/1520-0442(1999)012<0742:NHSTIP>2.0.CO;2
- Kageyama M and 9 others** (2021) The PMIP4 Last Glacial Maximum experiments: preliminary results and comparison with the PMIP3 simulations. *Climate of the Past* 17(3), 1065–1089. doi:10.5194/cp-17-1065-2021
- Kamleitner S and 7 others** (2022) The Ticino-Toce glacier system (Swiss-Italian Alps) in the framework of the alpine Last Glacial Maximum. *Quaternary Science Reviews* 279, 107400. doi:10.1016/j.quascirev.2022.107400
- Kamleitner S and 7 others** (2023) Last Glacial Maximum glacier fluctuations on the northern alpine foreland: geomorphological and chronological reconstructions from the Rhine and Reuss glacial systems. *Geomorphology* 423, 108548. doi:10.1016/j.geomorph.2022.108548
- Karger DN, Nobis MP, Normand S, Graham CH and Zimmermann NE** (2023) CHELSA-TraCE21k-high-resolution (1 km) downscaled transient temperature and precipitation data since the Last Glacial Maximum. *Climate of the Past* 19(2), 439–456. doi:10.5194/cp-19-439-2023
- Kelly J, Buoncristiani C and Schlüchter C** (2004) A reconstruction of the Last Glacial Maximum (LGM) ice surface geometry in the western Swiss Alps and contiguous alpine regions in Italy and France. *Eclogae Geologicae Helveticae* 0, 57–75. doi:10.1007/s00015-004-1109-6
- Khrulev C and the PISM Authors** (2022) PISM, a parallel ice sheet model: user's manual.
- Kutzbach J and Geuetter P** (1986) Influence of changing orbital parameters and surface boundary conditions on climate simulations for the past 18 000 years. *Journal of the Atmospheric Sciences* 43(16), 1726–1759. doi:10.1175/1520-0469(1986)043<1726:TIOCOP>2.0.CO;2
- Latombe G and 6 others** (2018) Comparison of spatial downscaling methods of general circulation model results to study climate variability during the Last Glacial Maximum. *Geoscientific Model Development* 11(7), 2563–2579. doi:10.5194/gmd-11-2563-2018
- Lingle CS and Clark JA** (1985) A numerical model of interactions between a marine ice sheet and the solid earth: application to a West Antarctic Ice Stream. *Journal of Geophysical Research: Oceans* 90(C1), 1100–1114. doi:10.1029/JC090iC01p01100
- Lofverstrom M, Caballero R, Nilsson J and Messori G** (2016) Stationary wave reflection as a mechanism for zonaling the Atlantic winter jet at the LGM. *Journal of the Atmospheric Sciences* 73(8), 3329–3342. doi:10.1175/JAS-D-15-0295.1
- Ludwig P, Pinto JG, Raible CC and Shao Y** (2017) Impacts of surface boundary conditions on regional climate model simulations of European climate during the Last Glacial Maximum. *Geophysical Research Letters* 44(10), 5086–5095. doi:10.1002/2017GL073622
- Luetscher M and 8 others** (2015) North Atlantic storm track changes during the Last Glacial Maximum recorded by Alpine speleothems. *Nature* 6, 6344. doi:10.1038/ncomms7344
- MacAyeal DR** (1997) EISMINT: lessons in ice-sheet modeling. *Department of Geophysical Sciences, University of Chicago, Chicago, IL* 1832, 1839.
- Merz N, Raible CC and Woollings T** (2015) North Atlantic Eddy-driven jet in interglacial and glacial winter climates. *Journal of Climate* 28(10), 3977–3997. doi:10.1175/JCLI-D-14-00525.1
- Messmer M, Gómez-Navarro JJ and Raible CC** (2017) Sensitivity experiments on the response of Vb cyclones to sea surface temperature and soil moisture changes. *Earth System Dynamics* 8(3), 477–493. doi:10.5194/esd-8-477-2017
- Mey J and 6 others** (2016) Glacial isostatic uplift of the European Alps. *Nature Communications* 7, 13382EP. doi:10.1038/ncomms13382

- Mix AC, Bard E and Schneider R (2001) Environmental processes of the ice age: land, oceans, glaciers (EPILOG). *Quaternary Science Reviews* **20**, 627–657. doi:10.1016/S0277-3791(00)00145-1
- Monegato G and 5 others (2007) Evidence of a two-fold glacial advance during the Last Glacial Maximum in the Tagliamento end moraine system (Eastern Alps). *Quaternary Research* **68**(2), 284–302. doi:10.1016/j.yqres.2007.07.002
- Monegato G, Scardia G, Hajdas I, Rizzini F and Piccin A (2017) The Alpine LGM in the boreal ice-sheets game. *Scientific reports* **7**(1), 1–8. doi:10.1038/s41598-017-02148-7
- Obrecht I and 5 others (2019) A critical reevaluation of palaeoclimate proxy records from loess in the Carpathian Basin. *Earth-Science Reviews* **190**, 498–520. doi:10.1016/j.earscirev.2019.01.020
- Palacios D, Hughes PD, Ruiz JMG and Andrés Nd (2021) *European glacial landscapes: maximum extent of glaciations*. Elsevier.
- Peltier WR, Argus DF and Drummond R (2015) Space geodesy constrains ice age terminal deglaciation: the global ICE-6G\_C (VM5a) model. *Journal of Geophysical Research: Solid Earth* **120**(1), 450–487. doi:10.1002/2014JB011176
- Powers JG and 9 others (2017) The weather research and forecasting model: overview, system efforts, and future directions. *Bulletin of the American Meteorological Society* **98**(8), 1717–1737. doi:10.1175/BAMS-D-15-00308.1
- Preusser F, Blei A, Graf H and Schlüchter C (2007) Luminescence dating of Würmian (Weichselian) proglacial sediments from Switzerland: methodological aspects and stratigraphical conclusions. *Boreas* **36**(2), 130–142. doi:10.1111/j.1502-3885.2007.tb01187.x
- Preusser F, Graf HR, Keller O, Krays E and Schlüchter C (2011) Quaternary glaciation history of northern Switzerland. *E&G Quaternary Science Journal* **60**(2–3), 282–305. doi:10.3285/eg.60.2-3.06
- Prömmel K, Cubasch U and Kaspar F (2013) A regional climate model study of the impact of tectonic and orbital forcing on African precipitation and vegetation. *Palaeogeography, Palaeoclimatology, Palaeoecology* **369**, 154–162. doi:10.1016/j.palaeo.2012.10.015
- Raible CC, Pinto JG, Ludwig P and Messmer M (2021) A review of past changes in extratropical cyclones in the northern hemisphere and what can be learned for the future. *Wiley Interdisciplinary Reviews – Climate Change* **12**(1), 1–21. doi:10.1002/wcc.680
- Ravazzi C, Badino F, Marsetti D, Patera G and Reimer PJ (2012) Glacial to paraglacial history and forest recovery in the Oglio glacier system (Italian Alps) between 26 and 15 ka cal BP. *Quaternary Science Reviews* **58**, 146–161. doi:10.1016/j.quascirev.2012.10.017
- Reber R and 9 others (2014) Timing of retreat of the Reuss Glacier (Switzerland) at the end of the Last Glacial Maximum. *Swiss Journal of Geosciences* **107**(2), 293–307. doi:10.1007/s00015-014-0169-5
- Ribolini A, Spagnolo M, Cyr AJ and Federici PR (2022) Last Glacial Maximum and early deglaciation in the Stura Valley, southwestern European Alps. *Quaternary Science Reviews* **295**, 107770. doi:10.1016/j.quascirev.2022.107770
- Roattino T and 6 others (2023) Paleogeographical reconstruction of the western French Alps foreland during the Last Glacial Maximum using cosmogenic exposure dating. *Quaternary Research* **111**, 68–83. doi:10.1017/qua.2022.25
- Roberts WHG, Li C and Valdes PJ (2019) The mechanisms that determine the response of the northern hemisphere's stationary waves to North American ice sheets. *Journal of Climate* **32**(13), 3917–3940. doi:10.1175/JCLI-D-18-0586.1
- Russo E and Cubasch U (2016) Mid-to-late holocene temperature evolution and atmospheric dynamics over Europe in regional model simulations. *Climate of the Past* **12**(8), 1645–1662. doi:10.5194/cp-12-1645-2016
- Russo E, Fallah B, Ludwig P, Karremann M and Raible CC (2022) The long-standing dilemma of European summer temperatures at the mid-Holocene and other considerations on learning from the past for the future using a regional climate model. *Climate of the Past* **18**(4), 895–909. doi:10.5194/cp-18-895-2022
- Russo E and 8 others (2023) High resolution LGM climate over Europe and the Alpine region using the regional climate model WRF. *EGU sphere* **2023**, 1–28. doi:10.5194/egusphere-2023-1197
- Schlüchter C (1991) Fazies und Chronologie des letzteiszeitlichen Eisaufbaues im Alpenvorland der Schweiz. In Fischer Frenzel B. G. (ed), *Klimageschichtliche Probleme der letzten 130000 Jahre*. New York: Stuttgart, pp. 401–407.
- Schmidt R, Weckström K, Lauterbach S, Tessadri R and Huber K (2012) North Atlantic climate impact on early late-glacial climate oscillations in the south-eastern Alps inferred from a multi-proxy lake sediment record. *Journal of Quaternary Science* **27**(1), 40–50. doi:10.1002/jqs.1505
- Seguinot J and 5 others (2018) Modelling last glacial cycle ice dynamics in the Alps. *The Cryosphere* **12**(10), 3265–3285. doi:10.5194/tc-12-3265-2018
- Seierstad IK and 9 others (2014) Consistently dated records from the Greenland GRIP, GISP2 and NGRIP ice cores for the past 104 ka reveal regional millennial-scale  $\delta^{18}O$  gradients with possible Heinrich event imprint. *Quaternary Science Reviews* **106**, 29–46. doi:10.1016/j.quascirev.2014.10.032
- Skamarock WC and 6 others (2008) A description of the advanced research WRF version 3. Technical Report TN-475+STR, National Center for Atmospheric Research (doi: 10.5065/D68S4MVH).
- Spötl C, Reimer PJ, Starnberger R and Reimer RW (2013) A new radiocarbon chronology of Baumkirchen, stratotype for the onset of the Upper Würmian in the Alps. *Journal of Quaternary Science* **28**(6), 552–558. doi:10.1002/jqs.2645
- Sutter J and 6 others (2019) Modelling the antarctic ice sheet across the mid-pleistocene transition – implications for oldest ice. *The Cryosphere* **13**(7), 2023–2041. doi:10.5194/tc-13-2023-2019
- Van Husen D (1987) *Die Ostalpen und ihr Vorland in der letzten Eiszeit (Würm)*. Geologische Bundesanstalt.
- van Husen D (2004) Quaternary glaciations in Austria. In Ehlers J and Gibbard P (eds), *Quaternary Glaciations Extent and Chronology Part I: Europe*, volume 2, Part 1 of *Developments in Quaternary Sciences*, Elsevier, pp. 1–13 (doi: 10.1016/S1571-0866(04)80051-4)
- Velasquez P, Messmer M and Raible CC (2020) A new bias-correction method for precipitation over complex terrain suitable for different climate states: a case study using WRF (version 3.8.1). *Geoscientific Model Development* **13**(10), 5007–5027. doi:10.5194/gmd-13-5007-2020
- Velasquez P, Kaplan JO, Messmer M, Ludwig P and Raible CC (2021) The role of land cover in the climate of glacial Europe. *Climate of the Past* **17**(3), 1161–1180. doi:10.5194/cp-17-1161-2021
- Velasquez P, Messmer M and Raible CC (2022) The role of ice-sheet topography on the Alpine hydro-climate at glacial times. *Climate of the Past* **18**(7), 1579–1600. doi:10.5194/cp-18-1579-2022
- Višnjić V, Herman F and Prasicsek G (2020) Climatic patterns over the European Alps during the LGM derived from inversion of the paleo-ice extent. *Earth and Planetary Science Letters* **538**, 116185. doi:10.1016/j.epsl.2020.116185
- Winkelmann R and 6 others (2011) The Potsdam Parallel Ice Sheet Model (PISM-PIK)–part 1: model description. *The Cryosphere* **5**(3), 715–726. doi:10.5194/tc-5-715-2011
- Wirsig C, Zasadni J, Christl M, Akçar N and Ivy-Ochs S (2016) Dating the onset of LGM ice surface lowering in the High Alps. *Quaternary Science Reviews* **143**, 37–50. doi:10.1016/j.quascirev.2016.05.001
- Wölfler A, Hampel A, Dielforder A, Hetzel R and Glotzbach C (2021) LGM ice extent and deglaciation history in the Gurktal and Lavantal Alps (eastern European Alps): first constraints from  $^{10}Be$  surface exposure dating of glacially polished quartz veins. *Journal of Quaternary Science* **37**(4), 677–687. doi:10.1002/jqs.3399
- Wu HB, Guiot JL, Brewer S and Guo ZT (2007) Climatic changes in Eurasia and Africa at the Last Glacial Maximum and mid-Holocene: reconstruction from pollen data using inverse vegetation modelling. *Climate Dynamics* **29**, 211–229. doi:10.1007/s00382-007-0231-3
- Wüthrich L and 9 others (2018)  $^{10}Be$  surface exposure dating of the last deglaciation in the Aare Valley, Switzerland. *Swiss Journal of Geosciences* **111**(1), 295–303. doi:10.1007/s00015-018-0298-3
- Zhu J and 10 others (2017) Reduced ENSO variability at the LGM revealed by an isotope-enabled Earth system model. *Geophysical Research Letters* **44**(13), 6984–6992. doi:10.1002/2017GL073406